Title Page

AEE788 Inhibits Basal Body Assembly and Blocks DNA Replication in the African Trypanosome[‡]

Catherine Sullenberger, Daniel Pique, Yuko Ogata, and Kojo Mensa-Wilmot.

Department of Cellular Biology, and Center for Tropical and Emerging Global Diseases, University of Georgia, Athens, GA (C.S., D.P., K. M-W.) and the Proteomics Facility, Fred Hutchinson Cancer Research Center, Seattle, WA (Y. O.).

Running Title: Chemical Biology of AEE788 in the African Trypanosome

Corresponding author: Kojo Mensa-Wilmot. Address: University of Georgia, Biological Sciences

Building 701, Athens, GA, 30602. E-mail: mensawil@uga.edu

Number of text pages: 57

Number of tables: 2

Number of Figures: 10

Number of References: 105

Number of words in Abstract: 243

Number of words in introduction: 699

Number of words in discussion: 1403

List of abbreviations:

BSA: bovine serum albumin

EdU: 5-ethynyl-2'-deoxyuridine

FAZ: flagellar attachment zone

GI_{50}: growth inhibitory concentration (by 50%)

HAT: human African trypanosomiasis

IC_{50}: inhibitory concentration (by 50%)

kDNA: kinetoplast DNA

NTD: neglected tropical disease

PFR: paraflagellar rod

PI: propidium iodide

Tf: transferrin

TL: tomato lectin

T_{10} = time at which 10% of the observed maximum is reached

T_{50} = time at which 50% of the observed maximum is reached

T_{90} = time at which 90% of the observed maximum is reached

Abstract

Trypanosoma brucei causes human African trypanosomiasis (HAT). The pyrrolopyrimidine AEE788 (a hit for anti-HAT drug discovery) associates with three trypanosome protein kinases. Herein we delineate the effects of AEE788 on *T. brucei* using chemical biology strategies. AEE788 treatment inhibits DNA replication in the kinetoplast (mitochondrial nucleoid) and nucleus. In addition, AEE788 blocks duplication of the basal body and the bilobe without affecting mitosis. Thus, AEE788 prevents entry into S phase of the cell division cycle. To study kinetics of early events in trypanosome division, we employed an "AEE788 block and release" protocol to stage entry into S phase. A time-course of DNA synthesis (nuclear and kinetoplast DNA (kDNA)), duplication of organelles (basal body, bilobe, kinetoplast, nucleus), and cytokinesis was obtained. Unexpected findings include the following: (i) basal body and bilobe duplication are concurrent, (ii) maturation of probasal bodies, marked by TbRP2 recruitment, is coupled with nascent basal body assembly, monitored by localization of TbSAS6 at newly forming basal bodies, and (iii) kinetoplast division is observed in G2, after completion of nuclear DNA synthesis. Prolonged exposure of trypanosomes to AEE788 inhibited transferrin endocytosis, altered cell morphology, and decreased cell viability. To discover putative effectors for AEE788's pleiotropic effects, proteome-wide changes in protein phosphorylation induced by the drug were determined. Putative effectors include an SR protein kinase, bilobe proteins, TbSAS4, TbRP2, and BILBO-1. Loss of function of one or more of these effectors can, from published literature, explain the polypharmacology of AEE788 on trypanosome biology.

Introduction

Trypanosoma brucei is a protozoan parasite that causes Human African Trypanosomiasis (HAT) (reviewed in (Kennedy, 2013; Lejon and Buscher, 2005)). Current HAT chemotherapies are administered by injection and have toxic side effects (reviewed in (Babokhov et al., 2013)), making them far from ideal. An attractive drug discovery approach for neglected tropical diseases (NTDs), such as HAT, is chemical scaffold repurposing (Patel et al., 2013). In this strategy, drugs with proven efficacy against other diseases are screened for activity against HAT, reducing time and cost associated with early-stage drug discovery (DiMasi et al., 2003). We identified a small molecule kinase inhibitor, AEE788 (Daniela Meco, 2010; Traxler et al., 2004), as a "hit" (GI_{50} = 2.5 µM) (Behera et al., 2014) for HAT drug discovery. Subsequently, AEE788 was established as an anti-trypanosomal lead drug (Behera et al., 2014). AEE788 forms complexes with three trypanosome protein kinases (Katiyar et al., 2013) suggesting that it is a multi-targeted antagonist or agonist (Dar and Shokat, 2011) whose toxicity to trypanosomes is likely based on exerting pleiotropic biological effects.

Stages of the trypanosome cell division cycle can be identified by enumeration of single copy organelles, including the kinetoplast (mitochondrial nucleoid containing kinetoplast DNA (kDNA)), basal body, and nucleus (Sherwin and Gull, 1989; Woodward and Gull, 1990). In G1, trypanosomes have a single round kinetoplast (K) and a single nucleus (1K1N) (Sherwin and Gull, 1989). As cells transition into S phase, synthesis of kDNA (reviewed in (Jensen and Englund, 2012)) is associated with kinetoplast elongation (Gluenz et al., 2011), generating early S phase cells with a single elongated kinetoplast (Ke) and one nucleus (1Ke1N) (Siegel et al., 2008). Division of the kinetoplast precedes mitosis forming a 2K1N population (Woodward and Gull, 1990). 2K2N trypanosomes are formed after mitosis which generate 1K1N cells following cytokinesis (Sherwin and Gull, 1989), completing the division cycle (reviewed in (Hammarton, 2007; Li, 2012; Zhou et al., 2014)).

The basal body is the microtubule-organizing center for the flagellar axoneme. Additionally, the basal body is attached to the kinetoplast (Ogbadoyi et al., 2003) and has a role in inheritance of the mitochondrial genome (Robinson and Gull, 1991). Accordingly, basal body biogenesis is tightly coordinated with the cell division cycle (Gluenz et al., 2011; Sherwin and Gull, 1989; Woodward and Gull, 1990). Prior to duplication, trypanosomes have a mature basal body adjacent to an immature probasal body (Sherwin and Gull, 1989). Maturation of the probasal body produces cells with two mature basal bodies, each of which seed a new probasal body (Gluenz et al., 2011; Lacomble et al., 2010; Sherwin and Gull, 1989). No quantitative time-course study of the conversion of putative intermediates into mature basal bodies has been reported.

The flagellum exits the trypanosome cell body via the flagellar pocket (Lacomble et al., 2009). Duplication of the flagellar pocket depends on basal body duplication and separation (Lacomble et al., 2010). Outside the cell body, the flagellar membrane is conjoined to the plasma membrane by the flagellar attachment zone (FAZ) (Kohl et al., 1999; Sherwin and Gull, 1989). Cytokinesis requires duplication of the flagellum and its associated cytoskeletal structures (Kohl et al., 2003; Robinson et al., 1995). The bilobe is a cytoskeletal structure closely associated with the FAZ filament (Esson et al., 2012) and is implicated in FAZ formation (Bangs, 2011; Zhou et al., 2010). The flagellar pocket is the major site of endocytosis, a process needed for nutrient uptake (reviewed in (Field et al., 2009)). Bloodstream trypanosomes require host transferrin (Tf), as a source of iron, for proliferation (Schell et al., 1991). Interestingly, trypanosome glycogen synthase kinase (TbGSK3ß), an AEE788-associated protein kinase (Katiyar et al., 2013), regulates Tf endocytosis (Guyett et al., 2016).

In our effort to understand the basis of AEE788 toxicity in *T. brucei*, we show that AEE788 blocks S phase entry of bloodstream trypanosomes, inhibits transferrin endocytosis, and alters cell morphology. Unexpectedly, we found that AEE788 could be used to enrich pre-S phase

trypanosomes. Using a novel "AEE788 block and release" protocol we document the kinetics of

DNA replication and subcellular organelle duplication in bloodstream trypanosomes. Finally, we

show that AEE788 perturbs phosphoprotein homeostasis, offering insight into the putative effector

proteins involved in AEE788-disrupted phospho-signaling pathways in the African trypanosome.

Materials and Methods

Parasite cultures

Bloodstream *T. brucei*, RUMP528 (Leal et al., 2001) or Lister 427, were cultured in HMI-9 medium supplemented with 10% Fetal Bovine Serum (Atlanta Biologicals; Flowery Branch, GA), 10% Serum Plus™ (SAFC Biosciences; Lenexa, KS) and 1% antibiotic-antimycotic solution (Corning; Corning, NY) at 37 °C, 5% CO_2 (Hirumi, 1994). For all experiments trypanosomes were harvested in logarithmic phase (i.e. less than 1 x 10^6 cells/ml).

Time-dependent inhibition of trypanosome proliferation at a cytostatic concentration of AEE788

T. brucei were resuspended at 5 x 10^5 cells/ml (5 ml), in a Corning 25 cm^2 culture flask, and treated with AEE788 (Novartis; Basel, Switzerland) to achieve a final concentration of 5 μM or equal volume (0.1%) of the drug solvent DMSO (Thermo Fisher; Waltham, MA). Cells were incubated at 37 °C, 5% CO_2. Trypanosome density was measured with a haemocytometer after 4 h, 9 h and 16 h of incubation. Both sides of the haemocytometer were counted twice and averaged for every time point. Biological replicates were performed twice.

DAPI staining of DNA in the kinetoplast and nucleus following AEE788 treatment

T. brucei (5 x 10^5 cells/ml) was treated with AEE788 (5 μM), or equal volume (0.1%) DMSO (drug solvent) for 4 h at 37 °C, 5% CO_2. Treated cells were pelleted (3000 x g for 5 min), resuspended in 1 ml of 4% paraformaldehyde (Affymetrix; Santa Clara, CA) in phosphate-buffered saline (Thermo Fisher), and incubated for 15 min at room temperature. Cells were pelleted by centrifugation, as described previously, and adhered to poly-L-lysine (Sigma Adlrich; St. Louis, MO) coated coverslips for 15 min. Coverslips were briefly washed with phosphate-buffered saline (PBS) before being mounted onto microscope slides with VectaSheild® Mounting Medium (Vector Labs; Burlingame, CA), containing 1.5 μM 4',6-diamidino-2-phenylindole (DAPI) to stain nuclear

and kinetoplast DNA. Trypanosomes were visualized with a high sensitivity interline camera on an EVOS fluorescence (EVOS® FL) microscope (Life Technologies; Grand Island, NY). The number of kinetoplasts and nuclei per cell, in 150 trypanosomes, were scored in four independent experiments.

Time-course for duplication of the kinetoplast and nucleus

Following a 4 h treatment with AEE788 (5 µM), trypanosomes were washed twice and resuspended in drug-free HMI-9 medium (5 x 10^5 cells/ml). Cells were returned to an incubator (37 °C, 5% CO_2) for 1 h, 2 h, 3 h, 4 h, 5 h or 6 h. Cells were fixed and stained with DAPI as described above. Trypanosomes (150) were scored based on their number of kinetoplasts and nuclei (n = 3 for each time point).

Detection of DNA synthesis with 5-ethynyl-2'-deoxyuridine (EdU)

Bloodstream trypanosomes (5 x10^5 cells/ml) were treated with AEE788 (5 µM) or DMSO (0.1%) for 4 h at 37 °C, 5% CO_2. EdU (5-ethynyl-2'-deoxyuridine) (300 µM) (Life Technologies), and 2'-deoxycytidine (200 µM) (Sigma Adlrich), were added to both DMSO and AEE788-treated samples 3.5 h into the 4 h treatment (i.e. 30 min labeling period). Following the 4 h incubation, cells were washed once in phosphate-buffered saline supplemented with 1% glucose (PBSG), fixed with 4% paraformaldehyde (PFA) in PBS (15 min), adhered to poly-L-lysine coated coverslips, and permeabilized with 0.5% Triton X-100 (Thermo Fisher) in PBS for 25 min at room temperature. Permeabilized trypanosomes were washed with PBS and incubated in the dark for 30 min in a click-iT reaction cocktail: 4 mM copper sulfate (Sigma Adlrich); 60 µM azide conjugated to Alexa Fluor® 488 (Life Technologies); 1 x Tris-buffered saline (20 mM Tris base (Genesee Scientific; San Diego, CA) and 0.14 M NaCl (Sigma Adlrich)); and 300 mM ascorbic acid (Avantor Performance Materials; Center Valley, PA). Cells were washed thrice in PBS (3 min each) before mounting with VectaSheild® Mounting Medium, containing DAPI (1.5 µM), onto microscope slides.

Cells were visualized by fluorescence microscopy on the Applied Precision DeltaVision II Microscope System (GE Healthcare; Issaquah, WA) on an Olympus IX-71 inverted microscope (Olympus; Center Valley, PA). Images were captured with a cooled CCD camera. The kinetoplast and nucleus of each trypanosome (n = 100-150) were characterized as EdU-positive or EdU-negative in three independent experiments.

Time-course of DNA synthesis

Trypanosomes were treated for 4 h with AEE788 (5 μM), washed twice and resuspended in drug-free HMI-9 medium (5 x 10^5 cells/ml). Trypanosome aliquots (2 x 10^6 cells) were harvested every hour over a three-hour time-course (1 h to 4 h post AEE788 washout) and incubated in medium containing EdU (300 μM) and 2'-deoxycytidine (200 μM) for 30 min (37 °C, 5% CO_2). Cells were subsequently processed as described above. Cells were first collected from 0 h – 4 h after AEE788 washout to identify the range of DNA synthesis. Subsequently trypanosomes were harvested from 0 h to 3 h post AEE788 wash off (n = 3) to monitor initiation of DNA synthesis. Additionally, cells were collected between 2 h – 4 h after AEE788 washout (n = 2) in attempts to detect termination of DNA synthesis. The kinetoplast and nucleus of 100-150 trypanosome were scored as EdU-positive or EdU-negative at each time point for all experiments (0 h and 2 h, n = 6; 1 h, n = 4; 3 h and 4 h, n = 3).

Immunofluorescence detection of basal bodies and bilobes

Trypanosomes (5 x 10^5 cells/ml) were treated with AEE788 (5 μM) or an equal volume (0.1%) of DMSO (drug solvent) for 4 h at 37 °C, 5% CO_2. Cells were washed once with PBSG, and adhered to poly-L-lysine coated coverslips for 5 min, quickly air-dried, and fixed with methanol (Thermo Fisher) for 20 min at -20 °C. Coverslips were briefly rinsed with PBS and rehydrated in blocking buffer (1% bovine serum albumin (BSA) (Sigma Aldrich) in PBS) for 1 h. Permeabilized trypanosomes were either co-stained with the primary antibodies YL1/2 (EMD Millipore; Billerica,

MA) (Andre et al., 2014) and anti-TbSAS6 (Hu et al., 2015a) to detect basal bodies or stained with 20H5 (EMD Millipore) (He et al., 2005) for bilobes. The TbSAS6 antibody was a generous gift from Dr. Ziyin Li (University of Texas Health Science Center). Antibodies were diluted (YL1/2 at 1:1000; anti-TbSAS6 and 20H5 at 1:500) in blocking buffer and incubated with cells for 1 h at room temperature. Cells were rinsed thrice, 5 minutes each, in PBS prior to exposure to the secondary antibody at a dilution of 1:2000 in blocking buffer for 1 h at room temperature: Alexa Fluor® 488 goat anti-rat and Alexa Fluor® 594 goat anti-rabbit or Alexa Fluor® 488 goat anti-mouse, respectively (Molecular Probes; Eugene, OR). Cells were rinsed three times, 5 minutes each, in PBS and mounted onto microscope slides with VectaSheild® Mounting Medium supplemented with DAPI (1.5 µM). Cells were then visualized with a DeltaVision Microscope System II, at the Biomedical Microscopy Core (BMC) at the University of Georgia, and images captured with a cooled CCD camera. The number of basal bodies and bilobes were quantitated in three independent experiments (100-150 trypanosome quantitated per experiment). Basal bodies were considered mature if they were co-labeled with YL1/2 and anti-TbSAS6 or if they were labeled by YL1/2 alone. Basal bodies labeled solely by anti-TbSAS6 were counted as probasal bodies.

Time-course of basal body and bilobe duplication

Trypanosomes (5×10^5 cells/ml) were treated with AEE788 (5 µM), for 4 h (37 °C, 5% CO_2), washed twice in drug-free HMI-9 medium and resuspended in drug-free medium. Cells were returned to the incubator for 0 h, 2 h, 2.5 h, 3 h or 3.5 h, collected and prepared for immunofluorescence assays as described above (YL1/2 and anti-TbSAS6 double labeling or 20H5 staining). The time-course was repeated in three independent experiments with the number of basal bodies (in YL1/2 and anti-TbSAS6 stained cells) and bilobes (in 20H5 stained cells) assessed in 100-150 trypanosomes at each time point for all experiments.

Analysis of time-course studies using nonlinear regression curve fitting

Nonlinear regression curves were applied to time-course data documenting the recovery of DNA synthesis and organelle duplication (kinetoplast, basal body, bilobe and nucleus) following an "AEE788 block and release" protocol (see above) using GraphPad Prism. GraphPad was used to calculate the time at which 50% (T_{50}) of the maximum activity (*e.g.* DNA synthesis) was achieved based on a sigmoidal function. Calculations for kinetoplast elongation (measured by the percentage of 1Ke1N cells) and cytokinesis (based on the reappearance of 1K1N cells) were based on time points between 0 h – 4 h, and 5 h – 6 h, respectively, when the minimum and maximum for these events were observed (a 3rd order polynomial nonlinear regression was used to show data trends for these events). Based on the T_{50} and the Hill slope (provided by GraphPad Prism), we calculated the time at which 10% (T_{10}) and 90% (T_{90}) of the maximum was achieved using the following equation provided by GraphPad Software: $T_x = ((x/100-x)^{1/H})T_{50}$ where H = Hill slope and x = the desired percentage (of maximum).

Assessment of cell viability following AEE788 treatment

Trypanosomes (5×10^5 cells/ml) were treated with AEE788 (5 µM) or equal volume (0.1%) DMSO (drug solvent) for 4 h, 9 h, or 16 h. Thereafter, cells from each treatment group (1 ml each) were aliquoted into 1.5 ml microcentrifuge tubes and treated with propidium iodide (3 µM) (Sigma Aldrich). Cells were immediately incubated on ice for 15 min and analyzed using a Beckman Coulter Cyan flow cytometer to measure propidium iodide fluorescence. FlowJo software (FlowJo, LLC; Ashland, OR) was used to gate live cell populations based on size and shape (forward and side scatter) and to quantitate the fluorescence intensity of propidium iodide in 10,000 trypanosomes (n = 2).

Evaluation of trypanosome endocytosis of transferrin (Tf), bovine serum albumin (BSA) and tomato lectin (TL)

Trypanosomes were treated with AEE788 (5 µM) or equal volume (0.1%) DMSO (drug solvent) for 9 h (37 °C, 5% CO_2). Cells were washed and resuspended in serum-free HMI-9 medium devoid of AEE788 or DMSO (5 x 10^5 cells/ml). Trypanosomes were incubated with fluorescent endocytic cargo for 15 min at 37 °C, 5% CO_2: 25 µg Tf-Alexa Fluor® 488 Conjugate (Thermo Fisher), 25 BSA labeled with Alexa Fluor® 647 (Thermo Fisher), or 10 µg DyLight® 488-TL (Vector Laboratories). Cells were subsequently transferred to an ice-water bath and washed with cold PBSG at 4 °C (3000 x g for 5 min). Cells were resuspended in 1 ml PBSG, with propidium iodide (3 µM), as a marker for non-viable cells, and analyzed on the Beckman Coulter Cyan flow cytometer. FlowJo software (FlowJo, LLC) was used to gate viable trypanosome populations, based on size, shape (forward and side scatter) and propidium iodide exclusion. Fluorescence intensity of endocytic cargo was measured only in viable cell populations (negative for propidium iodide uptake). FlowJo was then used to determine the median fluorescence intensity of each endocytic cargo in trypanosome populations (15,000 events, n = 3).

Quantitation of changes in trypanosome morphology

Trypanosomes (5 x 10^5 cells/ml) were treated with AEE788 (5 µM) or equal volume (0.1%) DMSO (drug solvent) for 4 h, 9 h, or 16 h. After each incubation period cells were transferred to a haemocytometer and visualized (live) with an EVOS XL Core microscope (Thermo Fisher). Cells (100/incubation period) were scored based on morphology in two independent experiments.

Immunofluorescence detection of the paraflagellar rod (PFR) and flagellum

Trypanosomes (5 x 10^5 cells/ml) were treated with DMSO or AEE788 for 16 h (37 °C, 5% CO_2), washed with PBSG and adhered to poly-L-lysine coated coverslips (5 min). Once adhered, cells were quickly air-dried and fixed with methanol for 20 min at -20 °C. Cells were rehydrated in blocking buffer (PBS supplemented with 1% BSA) for 1 h. Subsequently, trypanosomes were incubated with anti-PFR2 (1:500) and 20H5 (1:500) in blocking buffer for 1 h at room temperature.

The polyclonal rabbit antibody against PFR2 was generated by GenScript® (Piscataway Township, NJ). Trypanosomes were washed three times, 5 min each, in PBS before addition of fluorescent secondary antibodies (1:2000 in blocking buffer) for 1 h at room temperature (Alexa Fluor® 488 goat anti-rabbit or Alexa Fluor® 594 goat anti-mouse, respectively). Cells were washed three times in PBS, 5 min each, prior to mounting onto microscope slides with VectaSheild® Mounting Medium containing DAPI (1.5 µM). Cells were visualized by fluorescence microscopy on an Applied Precision DeltaVision II Microscope System (GE Healthcare; Issaquah, WA) with an Olympus IX-71 inverted microscope (Olympus; Center Valley, PA). Images were captured with a cooled CCD camera.

Scanning Electron Microscopy

T. brucei (5×10^5 cells/ml) were treated with AEE788 (5 µM) for 12 h in HMI-9 medium. Cells were centrifuged (1500 x g for 5 min) and washed with ice-cold PBSG. Cells were fixed with 2% glutaraldehyde in PBS for 1 h at room temperature, washed with PBS and adhered to poly-L-lysine coated coverslips. Cells on coverslips were treated with OsO_4 (1%) for 30 min at RT, washed thrice in water and dehydrated with increasing concentrations of ethanol by incubating them sequentially in 25%, 30%, 50%, 75%, 85%, 95%, and 100% ethanol for 5 min each. The samples were dried at critical point with a Tousimis Critical Point Dryer (Samdri-780 A), and sputter coated (gold) with an SPI Module Sputter Coater following standard protocols. Samples were viewed using a Zeiss 1450EP variable pressure scanning electron microscope at the Center for Advanced Ultrastructural Research (CAUR) at the University of Georgia.

Phosphopeptide enrichment and identification in AEE788-treated trypanosomes

Trypanosomes (5×10^5 cells/ml) were treated with either AEE788 (5 µM) or equivalent volume (0.1%) DMSO (drug solvent) at 37 ºC (4 h or 9 h). Trypanosomes (2×10^8 cells) were moved to ice, washed with cold PBSG containing 1X HALT Phosphatase Inhibitor Cocktail (PIC)(Thermo

Fisher), lysed by sonication in 50 mM HEPES (Thermo Fisher), pH 7.6, 8 M urea (Thermo Fisher),

4 mM DTT (Sigma Aldrich), 1X HALT PIC and alkylated with 9 mM iodoacetamide (Bio-Rad;

Hercules, CA) for 30 min (away from light). The lysate was diluted 5-fold with 50 mM HEPES, pH

7.6, and 1X HALT PIC (1.6 M urea final) followed by protein digestion with immobilized trypsin

agarose (Thermo Fisher) for 48 at room temperature. After collecting the beads by centrifugation,

the peptide supernatant was diluted 10-fold with 0.1% trifluoroacetic acid (TFA) (Thermo Fisher)

and desalted over a Sep-Pak C18 column (Waters; Milford MA). A step gradient of acetonitrile

(25% followed by 50%) (Thermo Fisher) was used to elute peptides. Eluates were dried via

vacuum centrifugation. Phosphopeptides were then enriched by $FeCl_3$ charged metal affinity

chromatography (IMAC) made in-house (Proteomics core at Fred Hutchinson Cancer Research

Center). Briefly, peptide samples were resuspended in 80% acetonitrile, 0.1% TFA and loaded

onto $FeCl_3$ charged IMAC resin (10 µl bed volume). The resin was washed three times with 150

µl of 80% acetonitrile in 0.1% TFA, then a final wash of 1% TFA (150 µl). The peptides were

eluted twice (3 min each) with 150 µl of 500 mM potassium phosphate (pH 7), and desalted using

ZipTip™ C18 (Millipore Corporation; Billerica, MA) before MS analysis.

LC-MS/MS analysis was performed with an Easy-nLC 1000 (Thermo Scientific) coupled to an

Orbitrap Elite mass spectrometer (Thermo Scientific). The LC system was configured in a vented

format (Licklider et al., 2002) consisting of a fused-silica nanospray needle (PicoTip™ emitter, 50

µm ID, New Objective) packed in-house (Fred Hutchinson Proteomics Facility) with Magic C18

AQ 100Å reverse-phase medium (Michrom Bioresources Inc.) (25 cm), and a trap (IntegraFrit™

Capillary, 100 µm ID, New Objective) containing Magic C18 AQ 200Å (2 cm). The peptide sample

was diluted in 10 µl of 2% acetonitrile and 0.1% formic acid in water and 8 µl was loaded onto the

column for separation using a two-mobile-phase system consisting of 0.1% formic acid in water

(A) and 0.1% acetic acid in acetonitrile (B). A 60 or 90-minute gradient from 7% to 35% acetonitrile

in 0.1% formic acid at a flow rate of 400 nl/minute was used for chromatographic separation. The

mass spectrometer was operated in a data-dependent MS/MS mode over the m/z range of 400-1800 at the 240,000 mass resolutions. For each cycle, the 20 most abundant ions from the scan were selected for MS/MS analysis using 35% normalized collision energy. Selected ions were dynamically excluded for 30 seconds.

Raw MS/MS data were analyzed with Proteome Discoverer software v 1.4 (Thermo Fisher) using SEQUEST (Eng et al., 1994) as a search engine against TriTrypDB database version 4.1 (from TritrypDB.org), which included common contaminants such as human keratin. The database contained 8,614 protein entries including contaminants. The following modifications were considered: carbamidomethylation of cysteine as a fixed modification; phosphorylation of serine, threonine, tyrosine, and oxidation of methionine as variable modifications. The enzyme was set to trypsin allowing up to 2 missed cleavages. The precursor and fragment mass tolerances were set to 10 ppm and 0.6 Da respectively. Search results were run through Percolator (Kall et al., 2007) for scoring. The results were filtered for peptides identified with a false discovery rate lower than 0.05. Phosphorylation sites were evaluated and probability values were calculated using phosphoRS v. 3.1 (Taus et al., 2011). Specific phosphorylation sites in Table 1 were assigned if the PhosphoRS probability for the site was 80% or greater.

Statistical Analysis

To quantitate the effect of AEE788 on organelle (basal body, bilobe, nucleus, kinetoplast) duplication and trypanosome morphology, the distribution of cells was grouped according to organelle content per trypanosome, or trypanosome shape after treatment with drug or DMSO. To determine if AEE788 caused statistically significant changes in these distributions we compared the distribution obtained after exposure to AEE788 to that observed after treatment with DMSO (*i.e.,* control) using the Pearson chi-squared test of independence ($\alpha = 0.0005$).

A two sample Student's t-test was used to compare the median fluorescence of endocytosed

cargo (measure of internalization) between DMSO and AEE788-treated cells ($\alpha = 0.005$).

Results

AEE788 inhibits kinetoplast duplication

Our primary objective in these studies was to characterize pharmacological effects of AEE788 on bloodstream trypanosomes. To achieve this goal it was necessary to work with higher cell densities, and therefore higher drug concentrations, than previously used in proliferation inhibition assays (Behera et al., 2014), to provide adequate numbers of trypanosomes for follow-up phenotypic evaluation. We first identified the optimal AEE788 concentration and treatment time for "mode of action" studies (conditions that inhibit proliferation without death, thereby providing an opportunity to characterize disrupted pathways in living cells). We found that AEE788 (5 μM) arrested proliferation between 4 h and 9 h of treatment, but beyond 9 h the drug caused cell density to decrease (Supplemental Figure 1). These data indicate that AEE788 halts bloodstream trypanosome division within a single duplication cycle (~6-7 h) (Ajoko and Steverding, 2015; Hesse et al., 1995).

One hypothesis to explain the inability of cells to proliferate in the presence of AEE788 (Supplemental Figure 1) is that trypanosomes fail to progress through a specific point in the division cycle. To determine if AEE788 interfered with the cell division cycle we used DAPI to quantitate the number of kinetoplasts and nuclei per cell. Following a 4 h incubation with AEE788 the proportion of trypanosomes with one round kinetoplast (1K) and a single nucleus (1N) increased, compared to control cells treated with DMSO (drug vehicle) (Figure 1A). Quantitation of the percentage of cells with each "karyotype" (i.e. number of kinetoplasts and nuclei) demonstrated that AEE788 caused a statistically significant change in the cell type distribution as compared to the control population ($p = 7.4 \times 10^{-19}$). The proportion of cells with a 1K1N configuration (*i.e.* G1 trypanosomes) increased from 52.2% to 78.2% (Figure 1B). Concomitantly, the percentage of cells in S phase (i.e 1Ke1N cells (Kaufmann et al., 2012; Siegel et al., 2008)) dropped from 28.6% to 9.8% (Figure 1B). A decrease in the percentage of 2K1N cells, from 13%

in the control (DMSO-treated) to 2.7%, after AEE788 treatment indicated that kinetoplast

duplication was blocked (Figure 1B). In contrast, the proportion of post-mitotic trypanosomes

(2K2N) was unchanged during the 4 h AEE788 treatment, implying that mitosis was not affected

(Figure 1B).

AEE788 prevents DNA synthesis in the kinetoplast and nucleus

Failure of the kinetoplast to elongate following AEE788 treatment (Figure 1) led us to hypothesize

that the drug impairs kinetoplast DNA (kDNA) synthesis. We tested this hypothesis by labeling

kinetoplast and nuclear DNA with a thymidine analog, 5-ethynyl-2'-deoxyuridine (EdU) (Cavanagh

et al., 2011), in the absence or presence of AEE788 (Figure 2A). EdU labeling was performed for

30 minutes to detect newly synthesized DNA. Unlike nuclear incorporation of EdU, which can be

visualized throughout the nucleus, kDNA incorporation of EdU is limited to the ends of the

kinetoplast DNA network (Figure 2A) where newly synthesized minicircles are attached (reviewed

in (Liu et al., 2005)).

In control trypanosomes (treated with DMSO) 23.8% incorporated EdU into the kDNA network

(proportional to the number of 1Ke1N cells (Figure 1B)), while only 5.5% of kinetoplasts in

AEE788-treated trypanosomes incorporated EdU (Figure 2B). The distribution of replicating and

non-replicating kinetoplasts was significantly altered, as compared to control trypanosomes, by

AEE788 treatment (p = 4.9 x 10^{-4}). Nuclear DNA synthesis was also inhibited by AEE788

treatment. Only 14% of AEE788-treated trypanosomes incorporated EdU in the nucleus

compared to 52.2% in the control (Figure 2C), leading to a statistically significant difference in the

distribution of S phase nuclei (p = 3.1 x 10^{-19}). Inhibition of DNA synthesis in both trypanosome

DNA-containing organelles suggests that AEE788 impairs entry into S phase of the cell cycle, as

the protein factors and DNA origins needed for DNA replication in the nucleus and kinetoplast

differ (reviewed in (Jensen and Englund, 2012; Povelones, 2014; Tiengwe et al., 2014)). In

DMSO-treated populations the percentage of cells synthesizing kDNA is approximately 50% of the proportion synthesizing nuclear DNA (Figures 2B-2C). This observation may be explained by the fact that: (i) the time-course of DNA synthesis differs between kDNA and chromosomal DNA (Figures 5B-5C) (Woodward and Gull, 1990); and (ii) the sensitivity of EdU detection is higher in the nucleus which contains more DNA (Borst et al., 1982).

Effect of AEE788 on duplication of the basal body and bilobe

Trypanosomes in G1 have a single mature basal body (mBB) paired with an immature probasal body (pBB) each containing TbSAS6. TbRP2 (recognized by the antibody YL1/2 (Andre et al., 2014)) is localized to transitional fibers, found only on mature basal bodies (Andre et al., 2014). Maturation of the pBB is thought to precede assembly of new ones (Gluenz et al., 2011; Ikeda and de Graffenried, 2012; Lacomble et al., 2010; Sherwin and Gull, 1989). Thus, trypanosomes with two mBBs lacking adjacent pBBs (2mBB/0pBB) are thought to arise first as intermediates in biogenesis of the organelle. Subsequently a new pBB is assembled adjacent to each mBB to form 2mBB/2pBB trypanosomes. Migration of each mBB/pBB pair away from each other correlates with scission of the kinetoplast (Gluenz et al., 2011; Lacomble et al., 2010; Robinson and Gull, 1991; Sherwin and Gull, 1989). Given that AEE788 blocked division of the kinetoplast (Figure 1) we hypothesized that the drug inhibited basal body duplication. We tested this possibility using immunofluorescence to detect the number of mBBs and pBBs per trypanosome (Figure 3A).

The distribution of basal bodies (i.e., number of mBBs or pBBs per cell), was skewed towards trypanosomes with unduplicated basal bodies (1mBB/1pBB) after AEE788 treatment (p = 1.3 x 10^{-18}). In a control population (exposed to DMSO) 35.5% of cells had one mBB and one pBB (1mBB/1pBB) (Figure 3B). This population doubled to 73.5% following a 4 h treatment with AEE788 (Figure 3B). Additionally, the fraction of trypanosomes with 2mBB/2pBB dropped from 54.2% in the control to 21.5% in AEE788-treated trypanosomes (Figure 3B). Infrequently

trypanosomes with 1mBB/0pBB or 2mBB/1pBB were detected, likely a staining artifact, and these populations remained the same after DMSO or AEE788 treatment (Figure 3B). The data indicates that in the presence of AEE788, targeting of TbRP2 to the second basal body fails, possibly due to (i) absence of new transitional fibers, and/or (ii) inability to deliver TbRP2 to newly matured basal bodies. Further, AEE788 prevents assembly of new TbSAS6-positive pBBs in the absence of TbRP2 recruitment (Figure 3B). Together, these data indicate that AEE788 inhibits basal body duplication by interfering with recruitment of proteins to the organelle.

Failure of AEE788-treated trypanosomes to synthesize DNA (Figure 2) indicated that the drug blocked entry of trypanosomes into S phase. The bilobe, a centrin-containing cytoskeletal structure at the base of the flagellum (Esson et al., 2012), is duplicated in S phase (Zhou et al., 2014). We postulated that because AEE788 prevented S phase entry (Figure 2) the drug would inhibit bilobe duplication. We tested this hypothesis by evaluating the effect of AEE788 on bilobe biogenesis using the antibody 20H5, which detects centrins at the bilobe and basal body (He et al., 2005) (Figure 4A). AEE788 increased the fraction of trypanosomes with one bilobe from 54.7% to 77.5%, and decreased the proportion of trypanosomes with two bilobes from 45.3% to 22.5% (Figure 4B); a significant change in the distribution of cells with unduplicated and duplicated bilobes ($p = 3.6 \times 10^{-9}$). We conclude that AEE788 prevents bilobe duplication.

A time-course for DNA synthesis, and duplication of cytoskeletal organelles during trypanosome division

Experimental measurement of the kinetics of organelle duplication during bloodstream division has been hampered by the technical difficulties of enriching a pre-S phase trypanosome populations (Archer et al., 2011; Forsythe et al., 2009; Kabani et al., 2010; Mutomba and Wang, 1996). Discovery that AEE788 causes a build-up of pre-S phase trypanosomes (Figures 2-4)

suggested that a "block-and-release" protocol using the drug might be valuable for time-course studies of organelle duplication during trypanosome division.

We first tested whether DNA synthesis would resume upon removal of AEE788 from the trypanosome culture, indicating re-entry into S phase. For this objective, trypanosomes were treated with AEE788 (5 µM) for 4 h, washed and resuspended in drug-free HMI-9 medium. Following AEE788 withdrawal, cell aliquots were obtained every hour and incubated with EdU (Cavanagh et al., 2011) for 30 minutes (1 h to 4 h post-AEE788 washout). During the first hour after AEE788 removal, the percentage of trypanosomes that incorporated EdU into the kinetoplast (or nucleus) was similar to that observed immediately following AEE788 treatment (Figures 5A-5C). However, by 2 h the percentage of cells with EdU-positive kinetoplasts increased from 5%, immediately following AEE788 washout, to 25% (Figures 5A-5B). Likewise, the number of nuclei which incorporated EdU increased from 12% to 35% (Figures 5A and 5C). Using a sigmoidal nonlinear regression curve, we estimated a time at which significant DNA synthesis (*i.e.* 10% of the observed maximum (4 h) for EdU-positive kinetoplasts or nuclei) had occurred, designated as T_{10}. Similarly, we defined the time by which the EdU-positive population increased to 50% (T_{50}) or 90% (T_{90}) compared to the observed maximum (4 h). Initiation of nuclear DNA synthesis (T_{10} = 1.1 h) and kDNA synthesis (T_{10} = 0.9 h) occurred at similar times following AEE788 removal. However, the T_{50} for kinetoplast EdU incorporation (1.5 h) was reached approximately 30 minutes earlier than that of nuclear incorporation (T_{50} = 2.1 h) and it terminated an hour before nuclear DNA synthesis (T_{90} = 2.1 h and 3 h, respectively) (Figures 5B and 5C). This data is consistent with kinetoplast S phase terminating prior to completion of nuclear DNA synthesis (Woodward and Gull, 1990). We next performed time-course experiments for duplication of the kinetoplast (Figure 5D), nucleus (Figure 5D), basal body (Figures 6A-6B), and bilobe (Figures 6D-6E).

Kinetoplast elongation (i.e. appearance of 1Ke1N trypanosomes) was observed between 1 h and 4 h post-AEE788 release (T_{10} = 1.4 h; T_{50} = 2.3 h; T_{90} = 3.3 h) (Figure 5D). From 1 h to 4 h the fraction of 1Ke1N trypanosomes increased from 5% to 35% (Figure 5D and Supplemental Figure 2). Correspondingly, by 4 h the 1K1N population was reduced from 77%, immediately following AEE788 withdrawal, to 39% (Figure 5D). Kinetoplast division (defined as an increase in the percentage of 2K1N trypanosomes) was observed between 3 h and 4 h when the 2K1N population increased from 5% to 18.2% (T_{10} = 3 h; T_{50} = 3.4 h; T_{90} = 3.9 h) (Figure 5D and Supplemental Figure 2). Mitosis was detectable between 4 h and 5 h with the number of 2K2N cells increasing from 2.7% to 17% (T_{10} = 3.9 h; T_{50} = 4.4; T_{90} = 5 h), indicating that mitosis can be completed within one hour (Figure 5D and Supplemental Figure 2). Between 5 h and 6 h the number of 1K1N trypanosomes increased (35.9% to 56.9%), with a simultaneous decrease in all other populations (Figure 5D), demonstrating the completion of cytokinesis and the cell division cycle. This data is consistent with the 6-7 h division time observed in bloodstream trypanosomes (Ajoko and Steverding, 2015; Hesse et al., 1995).

Basal bodies were co-stained using the antibody YL1/2 (for TbRP2-positive mature basal bodies (mBB) (Andre et al., 2014)) and anti-TbSAS6 for mBBs and immature probasal bodies (pBBs) (Hu et al., 2015a) (Figure 6A). Immediately following AEE788 withdrawal, the majority of trypanosomes (73.4%) had 1mBB/1pBB, with 25.3% containing 2mBB/2pBB (Figure 6B). Between 2 h and 3 h following AEE788 washout, the percentage of trypanosomes with 2mBB/2pBB increased from 24.4% to 56.6% (Figures 6A-6B). A nonlinear regression analysis indicated that trypanosomes with 2mBB/2pBB emerged 2.3 h (T_{10}) after AEE788 removal and reached the observed maximum by 2.7 h (T_{90}) (Figure 6B). Assuming pBB maturation occurs prior to new pBB assembly (Gluenz et al., 2011; Ikeda and de Graffenried, 2012; Lacomble et al., 2010; Sherwin and Gull, 1989), one would expect to detect trypanosomes with two mBBs but no probasal bodies (2mBB/0pBB). Surprisingly, we detected a small fraction of trypanosomes (>7%)

with 2mBB/0pBB (Figure 6B). In fact, the kinetics of TbRP2 recruitment (a marker for pBB maturation) and assembly of new pBBs (monitored by TbSAS6) were remarkably similar (Supplemental Figure 3). Our data suggest that TbRP2 recruitment to mBBs coincides with, and may be coordinated with, pBB assembly (Figure 6C).

Bilobe duplication was examined using the anti-centrin antibody 20H5 (He et al., 2005) (Figure 6D). During the first two hours after AEE788 washout, less than 30% of trypanosomes had two bilobes (Figure 6E). By 3 h hours 45% of trypanosomes had two bilobes (T_{10} = 2 h; T_{50} = 2.4 h; T_{90} = 2.6 h) (Figure 6E). Thus, bilobe duplication occurs between two and three hours after release from an AEE788 block, coincident with basal body duplication (Figure 7).

A summary of the time-course for organelle duplication after AEE788 washout (Figures 5 and 6) is presented in Figure 7 based on the calculated T_{10}, T_{50} and T_{90} for each event. Briefly, kDNA synthesis and nuclear DNA synthesis begin at similar times following AEE788 removal (T_{10} = 0.9 h and 1.1 h, respectively). Kinetoplast elongation (T_{10} = 1.4 h) is detected approximately 30 minutes after the start of kDNA synthesis and coincides with nuclear DNA synthesis (T_{50} = 2.3 h and 2.1 h, respectively). Basal body and bilobe duplication also occur during nuclear DNA synthesis (T_{50} = 2.5 h and 2.4 h, respectively). Termination of kDNA synthesis (T_{90} = 2.1 h) is detected approximately an hour prior to cessation of nuclear S phase (T_{90} = 3 h). The end of nuclear DNA synthesis marks the start of kinetoplast division (T_{10} = 3 h), which continues for one hour (T_{90} = 3.8). Mitosis is completed within one hour (T_{10} = 3.9 h; T_{90} = 5 h). Lastly cytokinesis occurs between 5 h and 6 h after trypanosomes have entered S phase.

Trypanocidal effects of AEE788 are associated with endocytosis defects and changes in cell morphology

The ability of trypanosomes to resume division after a 4 h treatment with AEE788 (Figures 5-6) indicated that trypanosomes did not commit to death during that period of treatment. However, between 9 h and 16 h of AEE788 treatment trypanosome density decreases (Supplemental Figure 1). Accordingly, we postulated that extended exposure to the drug was necessary to impair trypanosome viability. We tested this idea by staining trypanosomes with propidium iodide (PI) which will not enter trypanosomes with an intact plasma membrane (Garner DI Fau - Pinkel et al., 1986). By 4 h, a small proportion of PI-positive trypanosomes (< 0.4%) was observed in the control group (exposed to DMSO) as well as those treated with AEE788 (Figure 8). After 9 h of drug treatment, however, 16.5% of AEE788-treated trypanosomes (compared to 1.5% in the DMSO-treated control) were positive for PI uptake, and by 16 h half of the population stained with PI (Figure 8). We conclude that beyond 9 h of treatment, AEE788 (5 μM) decreases trypanosome viability.

AEE788 associates with three trypanosome protein kinases (Katiyar et al., 2013). As such the drug is likely to exert pleiotropic effects on trypanosome biology as a multi-targeted kinase modulator. One AEE788-associated protein, TbGSK3ß (Katiyar et al., 2013), regulates transferrin endocytosis (Guyett et al., 2016). We therefore tested if AEE788 (5 μM) affected trypanosome endocytic pathways. Ligands internalized through glycosylphosphatidylinositiol (GPI) anchored-receptors, such as the transferrin receptor (Steverding et al.), follow a distinct endocytic pathway (Pal et al., 2002). We studied the effect of AEE788 treatment on internalization of three endocytic cargos. Transferrin was used for receptor-mediated endocytosis; bovine serum albumin (BSA) was a marker for bulk-phase endocytosis (Guyett et al., 2016; Morriswood and Schmidt, 2015); and tomato lectin (TL) was used to evaluate internalization of carbohydrate-binding proteins (Field et al., 2004; Nolan et al., 1999). Fluorescent cargo was used to monitor endocytosis following a 9 h treatment with DMSO (drug solvent) or AEE788 (washed off prior to incubation with cargo). Propidium iodide exclusion was used to gate for viable cells (Figure 9A) before fluorescence

intensity of endocytic cargo was measured (Figures 9B-9D). Based on the median fluorescence intensity, AEE788 decreased transferrin endocytosis by 87% (Figure 9B) (p = 2.8 x 10^{-3}), but increased BSA internalization by 40% (Figure 9C) (p = 3.1 x 10^{-3}), without affecting TL uptake (Figure 9D) (p = 0.9). Each cargo demonstrated a unique distribution of fluorescence intensity (proportional to the amount of cargo internalized) within the population (Figures 9B-9D). For reasons that are unclear to us, AEE788 broadened the distribution of fluorescence associated with BSA or TL internalization (Figures 9C-9D). These results demonstrate that trypanosomes are metabolically active after 9 h of exposure to AEE788, and that transferrin endocytosis is selectively inhibited.

AEE788 caused morphological changes in trypanosomes in a time-dependent manner (Figure 10A). Most trypanosomes had normal morphology following a 4 h treatment with AEE788 (5 µM). However, by 9 h the distribution of trypanosomes with altered morphology or normal shape shifted towards swollen and rounded cells, compared to that found after 4 h of AEE788 treatment (p = 6.6 x 10^{-17}). By 16 h the majority of AEE788-treated trypanosomes had changed morphology, compared to trypanosomes after a 4 h treatment (p = 1.1 x 10^{-64}) or after the 9 h treatment (p = 5.6 x 10^{-25}). Flagella of rounded trypanosomes were not observed by light microscopy (Figure 10A). Despite this fact, no detached flagella were detected in the culture medium. This fact prompted us to use alternative methods to detect flagella on rounded trypanosomes. Employing markers for the flagellum (anti-centrin antibody 20H5 (de Graffenried et al., 2013)) and paraflagellar rod (Portman and Gull, 2010) (anti-PFR2) we detected flagella juxtaposed to the periphery of rounded trypanosomes (Figure 10B). The presence of flagella outside rounded trypanosomes was confirmed by scanning electron microscopy (Figure 10C).

Changes in phosphoprotein homeostasis in AEE788-treated trypanosomes

The presence of AEE788 in complexes with trypanosome protein kinases (Katiyar et al., 2013) prompted us to determine whether AEE788 could alter phosphoprotein homeostasis in the parasite. We used IMAC enrichment of phosphopeptides, combined with LC-MS/MS, to identify changes in the abundance of protein phosphorylation following trypanosome exposure to AEE788. Because there are phenotypic differences associated with short-term (4 h) as compared to long-term (9 h) AEE788 treatment, we examined trypanosome phosphopeptides obtained after both treatment times. A total of 244 trypanosome peptides (176 unique proteins) showed a 2-fold, or greater, change in phosphorylation after AEE788 treatment (Supplemental Table 1), confirming that AEE788 influences protein phosphorylation in *T. brucei*.

After 4 h of AEE788 treatment, 56 unique trypanosome peptides showed decreased phosphorylation and 21 demonstrated increased phosphorylation (Supplemental Table 1). Proteins with decreased phosphorylation after 4 h of AEE788 treatment include a serine-arginine protein kinase (SRPK) (reviewed in (Giannakouros et al., 2011)), TbSAS4 (Hu et al., 2015b) and a bilobe protein (Morriswood et al., 2013) (Table 1). Proteins with increased phosphorylation include a protease (calpain-like cysteine peptidase) (Table 1).

After 9 h of AEE788 (5 μM) treatment, 115 trypanosome peptides with decreased phosphorylation and 52 peptides with increased phosphorylation were identified (Supplemental Table 1). Thus, extended exposure to AEE788 affected more peptides (167) than the 4 h treatment (77). Proteins with decreased phosphorylation following a 9 h exposure to AEE788 include a NIMA-related kinase (NEK) (reviewed in (Fry et al., 2012)), the basal body protein TbRP2 (Andre et al., 2014), a bilobe protein (Morriswood et al., 2013) and a flagellar pocket protein BILBO-1 (Bonhivers et al., 2008) (Table 2). Proteins with increased phosphorylation include a Tb14-3-3-associated kinase (TbAKB1 (Inoue et al., 2015)), a bilobe protein (Morriswood et al., 2013), and a ubiquitin-transferase (Table 2).

In some cases, the abundance of the phosphorylated peptide, as well as, the abundance of the parent protein (number in parentheses of Tables 1-2) changed. In most cases the magnitude of change in phosphopeptide abundance exceeds that observed for total protein abundance (*e.g.*, Tb427.01.2100 (Table 1) and Tb427.03.3080 (Table 2)). This data may indicate that phosphorylation influences stability of some trypanosome proteins, as observed in other eukaryotes (Ishida et al., 2000; Ulery et al., 2006; Vazquez et al., 2000; Wang et al., 2014; Yamamoto et al., 1999). Additionally, the altered phosphorylation of proteins involved in protein degradation (Table 1, Table 2 and Supplemental Table 1) may influence protein abundance.

Discussion

A new tool for identification of S phase regulators in bloodstream trypanosomes

S phase is the period of DNA synthesis by the replisome (reviewed in (Machida and Dutta, 2005)). DNA replication is restricted to S phase to ensure that the genome is replicated only once per division cycle (Nishitani and Lygerou, 2002). Kinetoplastids are early branching eukaryotes with a divergent genome (Berriman et al., 2005; Parsons et al., 2005) and signaling pathways responsible for entry into S phase are not fully defined in bloodstream trypanosomes (reviewed in (Tiengwe et al., 2014)). In higher eukaryotes the Dbf4-dependent kinase (DDK) (Sheu and Stillman, 2006; Sheu and Stillman, 2010; Zou and Stillman, 2000) and S phase cyclin dependent kinase (S-CDK) (Tanaka et al., 2007; Zou and Stillman, 2000) promote initiation of DNA synthesis. Trypanosomes lack homologs of the DDK complex, and trypanosome homologs to cyclin-dependent kinases (TbCRKs), do not regulate DNA replication in bloodstream trypanosomes; knockdown of TbCRK1 and TbCRK2 arrests procyclic (insect stage) trypanosomes in G1, but does not prevent DNA synthesis in bloodstream trypanosomes (Tu et al., 2005; Tu and Wang, 2004; Tu and Wang, 2005).

AEE788 prevents trypanosome entry into S phase by inhibiting DNA synthesis in the kinetoplast and nucleus (Figure 2). Accordingly, by combining our phenotypic analysis with the identification of AEE788-affected phosphoproteins (Supplemental Table 1) we envision the use of AEE788 as a small-molecule tool to identify novel proteins (from effectors of the drug's action observed at 4 h (Supplemental Tables 1A-1C)) that regulate S phase entry in bloodstream trypanosomes. In this strategy, proteins that are dephosphorylated (or hyperphosphorylated) will be knocked down (or overexpressed) genetically to determine their effect on DNA synthesis.

Kinetics of organelle duplication and protein recruitment to the basal body during trypanosome division

A novel strategy using AEE788 in a "block and release" protocol was used to enrich pre-S phase trypanosomes and to study the time-course of organelle duplication in the bloodstream stage parasites (Figures 5-7). Previous studies of basal body duplication in insect stage trypanosomes identified two groups of 1Ke1N cells based on probasal body formation: (i) 1Ke1N cells with two mBBs each lacking a pBB (*i.e.,* 2mBB/0pBB); and (ii) 1Ke1N cells with two mBBs paired with adjacent pBBs (*i.e.,* 2mBB/2pBB) (Gluenz et al., 2011; Ikeda and de Graffenried, 2012; Lacomble et al., 2010; Sherwin and Gull, 1989). In our quantitation of SAS6/RP2 double-labeled basal bodies, we found less than 7% of trypanosomes with 2mBB/0pBB (Figure 6B). The data indicates that 2mBB/0pBB is not a major intermediate for basal body duplication in bloodstream trypanosomes (Figure 6C). This conclusion is reinforced by our observation that during duplication of basal bodies, TbRP2 is recruited to mBBs with the same kinetics as TbSAS6 localization at nascent pBBs (Figure 6B and Supplemental Figure 3). Hence, recruitment of TbRP2 to mBBs is concurrent with new pBB formation. Our observations establish the utility of AEE788 as a small-molecule tool for monitoring the order of protein recruitment during basal body biogenesis (and perhaps of other cytoskeletal organelles).

Our data additionally provides new insight on the sequence of S phase events; DNA replication, with respect to organelle duplication in bloodstream trypanosomes. We found that kinetoplast elongation occurs throughout nuclear DNA synthesis, consistent with the annotation of 1Ke1N trypanosomes as S phase cells (Siegel et al., 2008) (Figure 7). Second, duplication of the basal body and bilobe are coincident (consistent with the idea of a continuous cytoskeletal network containing both organelles (Gheiratmand et al., 2013)). Duplication of these cytoskeletal structures occurs after kDNA synthesis, but is concurrent with nuclear S phase and kinetoplast elongation (both of which initiate approximately 30 minutes prior to duplication of the basal body and bilobe) (Figure 7). Third, kinetoplast division does not occur immediately after kDNA synthesis, but is observed one hour after termination of kDNA replication. During the intervening

period the basal body is duplicated. This lag between kDNA replication and kinetoplast division may reflect (i) a requirement of two basal bodies to facilitate kinetoplast fission (Lacomble et al., 2010; Robinson and Gull, 1991), (ii) a slow assembly of factors needed for kinetoplast division, or both. Nuclear DNA synthesis was completed before kinetoplast division (Figure 7), revealing that 2K1N trypanosomes are most likely in G2, in accordance with previous work (Siegel et al., 2008; Woodward and Gull, 1990). Mitosis was observed one hour after replication of the nuclear genome, implying that the trypanosome G2 lasts one hour during which kinetoplast division occurs.

Selective inhibition of endocytosis by AEE788

Extended AEE788 treatment (9 h) of trypanosomes inhibited transferrin endocytosis (Figure 9B). Interestingly, not all trypanosome endocytic pathways were affected by AEE788 treatment. Internalization of BSA, a marker for fluid phase endocytosis (Morriswood and Schmidt, 2015), was increased after AEE788 treatment (Figure 9C). A similar effect was observed after knockdown of TbGSK3ß (Guyett et al., 2016). Future studies will address the basis of AEE788's ability to selectively inhibit transferrin endocytosis (Figure 9) by knocking down (or overexpressing) putative effectors of the drugs action (Table 2, Supplemental Tables 1B and 1D).

Putative effectors of AEE78 action

AEE788 treatment of trypanosomes caused dephosphorylation of some proteins, but resulted in hyperphosphorylation of others (Tables 1-2 and Supplemental Table 1). Small molecule kinase inhibitors can paradoxically lead to hyperphosphorylation of proteins (Holderfield et al., 2013; Okuzumi et al., 2009) through a variety of mechanisms including; protection of their target from protein phosphatases (Gould et al., 2011), increasing (Zhang et al., 2003) or decreasing (Holderfield et al., 2013) inhibitory autophosphorylation, and activation of negative feedback loops (Wan et al., 2007).

Proteins with altered phosphorylation after 4 h of AEE788 treatment (Table 1) may be involved in biological pathways disrupted during short-term AEE788 exposure (4 h). They might be effectors for S phase entry (Figure 2) or duplication of the basal body (Figure 3) and bilobe (Figure 4). Of note, a cytoskeletal protein TbSAS4 and a bilobe protein (Tb427.10.3010 (Morriswood et al., 2013)) were dephosphorylated (Table 1). In other organisms SAS4 is a centriolar protein (Hodges et al., 2010) with essential roles in centriole duplication (Gogendeau et al., 2011; Leidel and Gönczy, 2003; Novak et al., 2016; Pelletier et al., 2006; Schmidt et al., 2009). The role of TbSAS4 in bloodstream trypanosomes remains to be explored.

Extended exposure (9 h) of trypanosomes to AEE788 inhibited transferrin endocytosis (Figure 9) and distorted cell morphology (Figure 10). These phenotypes may be explained by postulating that two proteins with altered phosphorylation, namely, Tb14-3-3-associated protein kinase (TbAKB1 (Inoue et al., 2015)) (Table 2) and BILBO-1 (Bonhivers et al., 2008) (Table 2), are effectors of AEE788 action. Knockdown of Tb14-3-3 reduces the size of recycling endosomes (Benz et al., 2010), and knockdown of BILBO-1 causes rounding of bloodstream trypanosomes (Bonhivers et al., 2008), comparable to the morphology of *T. brucei* observed after prolonged AEE788 treatment (Figure 10).

The relative abundance of phosphopeptides in DMSO-treated cells (drug vehicle control) and AEE788-treated trypanosomes was determined by spectral counting of LC-MS/MS data. Spectral counting (reviewed in (Lundgren et al., 2010)) has been used to document changes in protein expression (Kislinger et al., 2006; Old et al., 2005; Takadate et al., 2013) and phosphorylation (Dammer et al., 2015; Singec et al., 2016; Xie et al., 2010). However, there are limitations associated with this method: the dynamic range is poor for proteins of low abundance (Old et al., 2005). Additionally, reproducibility of data may be compromised by non-identical sampling of

peptides between instrument runs (*e.g.,* control versus experimental). The latter issue is mitigated by replicate runs and statistical analysis to improve confidence in identifying changes in protein levels between controls and experimental samples. Zhang et al showed that the Student's t-test offers the lowest false positive rate ($> 1\%$) for triplicate replicates (used in our analysis) when the fold-change in spectra is greater than two (Zhang et al., 2006). We reported proteins which were observed in three independent experiments and showed a statistically significant change in levels of phosphorylation as determined by Student's t-tests.

The functions of many phosphoproteins affected by AEE788 are unknown in bloodstream trypanosomes. Hence correlation of their dephosphorylation with the disruption of essential physiological trypanosome pathways, generates hypotheses as to the function of these uncharacterized phosphoproteins. In the future, we will focus on determining the role of these unstudied proteins in: (i) AEE788-perturbed pathways (Figures 2-4 and 9-10); and (ii) how their phosphorylation may modulate their biological functions.

Acknowledgments

Authorship Contributions

Research design: Mensa-Wilmot, Sullenberger, and Pique

Manuscript writing: Mensa-Wilmot and Sullenberger

Conducted experiments: Sullenberger and Ogata

References

Ajoko C and Steverding D (2015) A cultivation method for growing bloodstream forms of Trypanosoma brucei to higher cell density and for longer time. *Parasitology research* **114**(4): 1611-1612.

Andre J, Kerry L, Qi X, Hawkins E, Drizyte K, Ginger ML and McKean PG (2014) An alternative model for the role of RP2 protein in flagellum assembly in the African trypanosome. *The Journal of biological chemistry* **289**(1): 464-475.

Archer SK, Inchaustegui D, Queiroz R and Clayton C (2011) The cell cycle regulated transcriptome of Trypanosoma brucei. *PloS one* **6**(3): e18425.

Babokhov P, Sanyaolu AO, Oyibo WA, Fagbenro-Beyioku AF and Iriemenam NC (2013) A current analysis of chemotherapy strategies for the treatment of human African trypanosomiasis. *Pathog Glob Health* **107**(5): 242-252.

Bangs JD (2011) Replication of the ERES:Golgi junction in bloodstream-form African trypanosomes. *Molecular microbiology* **82**(6): 1433-1443.

Behera R, Thomas SM and Mensa-Wilmot K (2014) New Chemical Scaffolds for Human African Trypanosomiasis Lead Discovery from a Screen of Tyrosine Kinase Inhibitor Drugs. *Antimicrobial agents and chemotherapy*.

Benz C, Engstler M, Hillmer S and Clayton C (2010) Depletion of 14-3-3 proteins in bloodstream-form Trypanosoma brucei inhibits variant surface glycoprotein recycling. *International journal for parasitology* **40**(5): 629-634.

Berriman M, Ghedin E, Hertz-Fowler C, Blandin G, Renauld H, Bartholomeu DC, Lennard NJ, Caler E, Hamlin NE, Haas B, Bohme U, Hannick L, Aslett MA, Shallom J, Marcello L, Hou L, Wickstead B, Alsmark UC, Arrowsmith C, Atkin RJ, Barron AJ, Bringaud F, Brooks K, Carrington M, Cherevach I, Chillingworth TJ,

Churcher C, Clark LN, Corton CH, Cronin A, Davies RM, Doggett J, Djikeng A, Feldblyum T, Field MC, Fraser A, Goodhead I, Hance Z, Harper D, Harris BR, Hauser H, Hostetler J, Ivens A, Jagels K, Johnson D, Johnson J, Jones K, Kerhornou AX, Koo H, Larke N, Landfear S, Larkin C, Leech V, Line A, Lord A, Macleod A, Mooney PJ, Moule S, Martin DM, Morgan GW, Mungall K, Norbertczak H, Ormond D, Pai G, Peacock CS, Peterson J, Quail MA, Rabbinowitsch E, Rajandream MA, Reitter C, Salzberg SL, Sanders M, Schobel S, Sharp S, Simmonds M, Simpson AJ, Tallon L, Turner CM, Tait A, Tivey AR, Van Aken S, Walker D, Wanless D, Wang S, White B, White O, Whitehead S, Woodward J, Wortman J, Adams MD, Embley TM, Gull K, Ullu E, Barry JD, Fairlamb AH, Opperdoes F, Barrell BG, Donelson JE, Hall N, Fraser CM, Melville SE and El-Sayed NM (2005) The genome of the African trypanosome Trypanosoma brucei. *Science* **309**(5733): 416-422.

Bonhivers M, Nowacki S, Landrein N and Robinson DR (2008) Biogenesis of the trypanosome endo-exocytotic organelle is cytoskeleton mediated. *PLoS Biol* **6**(5): e105.

Borst P, van der Ploeg M, van Hoek JF, Tas J and James J (1982) On the DNA content and ploidy of trypanosomes. *Molecular and biochemical parasitology* **6**(1): 13-23.

Cavanagh BL, Walker T, Norazit A and Meedeniya AC (2011) Thymidine analogues for tracking DNA synthesis. *Molecules* **16**(9): 7980-7993.

Dammer EB, Lee AK, Duong DM, Gearing M, Lah JJ, Levey AI and Seyfried NT (2015) Quantitative Phosphoproteomics of Alzheimer's Disease Reveals Crosstalk between Kinases and Small Heat Shock Proteins. *Proteomics* **15**(0): 508-519.

Daniela Meco TS, Gian Franco Zannoni, Enrica Marinelli, Maria Grazia Prisco, Chiara de Waure and Riccardo Riccardi (2010) Dual inhibitor AEE788 reduces tumor growth in preclinical models of medulloblastoma. *Translational oncology* **3**: 326-335.

Dar AC and Shokat KM (2011) The evolution of protein kinase inhibitors from antagonists to agonists of cellular signaling. *Annu Rev Biochem* **80**: 769-795.

de Graffenried CL, Anrather D, Von Raussendorf F and Warren G (2013) Polo-like kinase phosphorylation of bilobe-resident TbCentrin2 facilitates flagellar inheritance in Trypanosoma brucei. *Molecular biology of the cell* **24**(12): 1947-1963.

DiMasi JA, Hansen RW and Grabowski HG (2003) The price of innovation: new estimates of drug development costs. *Journal of Health Economics* **22**(2): 151-185.

Eng JK, McCormack AL and Yates JR (1994) An approach to correlate tandem mass spectral data of peptides with amino acid sequences in a protein database. *Journal of the American Society for Mass Spectrometry* **5**(11): 976-989.

Esson HJ, Morriswood B, Yavuz S, Vidilaseris K, Dong G and Warren G (2012) Morphology of the trypanosome bilobe, a novel cytoskeletal structure. *Eukaryotic cell* **11**(6): 761-772.

Field MC, Allen CL, Dhir V, Goulding D, Hall BS, Morgan GW, Veazey P and Engstler M (2004) New approaches to the microscopic imaging of Trypanosoma brucei. *Microsc Microanal* **10**(5): 621-636.

Field MC, Lumb JH, Adung'a VO, Jones NG and Engstler M (2009) Chapter 1 Macromolecular Trafficking and Immune Evasion in African Trypanosomes. **278**: 1-67.

Forsythe GR, McCulloch R and Hammarton TC (2009) Hydroxyurea-induced synchronisation of bloodstream stage Trypanosoma brucei. *Molecular and biochemical parasitology* **164**(2): 131-136.

Fry AM, O'Regan L, Sabir SR and Bayliss R (2012) Cell cycle regulation by the NEK family of protein kinases. *Journal of cell science* **125**(Pt 19): 4423-4433.

Garner Dl Fau - Pinkel D, Pinkel D Fau - Johnson LA, Johnson La Fau - Pace MM and Pace MM (1986) Assessment of spermatozoal function using dual fluorescent staining and flow cytometric analyses. (0006-3363 (Print)).

Gheiratmand L, Brasseur A, Zhou Q and He CY (2013) Biochemical characterization of the bi-lobe reveals a continuous structural network linking the bi-lobe to other single-copied organelles in Trypanosoma brucei. *The Journal of biological chemistry* **288**(5): 3489-3499.

Giannakouros T, Nikolakaki E, Mylonis I and Georgatsou E (2011) Serine-arginine protein kinases: a small protein kinase family with a large cellular presence. *The FEBS journal* **278**(4): 570-586.

Gluenz E, Povelones ML, Englund PT and Gull K (2011) The kinetoplast duplication cycle in Trypanosoma brucei is orchestrated by cytoskeleton-mediated cell morphogenesis. *Molecular and cellular biology* **31**(5): 1012-1021.

Gogendeau D, Hurbain I, Raposo G, Cohen J, Koll F and Basto R (2011) Sas-4 proteins are required during basal body duplication in Paramecium. *Molecular biology of the cell* **22**(7): 1035-1044.

Gould CM, Antal CE, Reyes G, Kunkel MT, Adams RA, Ziyar A, Riveros T and Newton AC (2011) Active site inhibitors protect protein kinase C from dephosphorylation and stabilize its mature form. *The Journal of biological chemistry* **286**(33): 28922-28930.

Guyett PJ, Xia S, Swinney DC, Pollastri MP and Mensa-Wilmot K (2016) Glycogen Synthase Kinase 3β Promotes the Endocytosis of Transferrin in the African Trypanosome. *ACS Infectious Diseases* **2**(7): 518-528.

Hammarton TC (2007) Cell cycle regulation in Trypanosoma brucei. *Molecular and biochemical parasitology* **153**(1): 1-8.

He CY, Pypaert M and Warren G (2005) Golgi duplication in Trypanosoma brucei requires Centrin2. *Science* **310**(5751): 1196-1198.

Hesse F, Selzer PM, Muhlstadt K and Duszenko M (1995) A novel cultivation technique for long-term maintenance of bloodstream form trypanosomes in vitro. *Molecular and biochemical parasitology* **70**(1-2): 157-166.

Hirumi HHaK (1994) Axenic Culture of Arican Trypanosome Bloodstream Forms. *Parasitology today* **10**(2): 80-84.

Hodges ME, Scheumann N, Wickstead B, Langdale JA and Gull K (2010) Reconstructing the evolutionary history of the centriole from protein components. *Journal of cell science* **123**(Pt 9): 1407-1413.

Holderfield M, Merritt H, Chan J, Wallroth M, Tandeske L, Zhai H, Tellew J, Hardy S, Hekmat-Nejad M, Stuart DD, McCormick F and Nagel TE (2013) RAF inhibitors activate the MAPK pathway by relieving inhibitory autophosphorylation. *Cancer Cell* **23**(5): 594-602.

Hu H, Liu Y, Zhou Q, Siegel S and Li Z (2015a) The Centriole Cartwheel Protein SAS-6 in Trypanosoma brucei Is Required for Probasal Body Biogenesis and Flagellum Assembly. *Eukaryotic cell* **14**(9): 898-907.

Hu H, Zhou Q and Li Z (2015b) SAS-4 Protein in Trypanosoma brucei Controls Life Cycle Transitions by Modulating the Length of the Flagellum Attachment Zone Filament. *The Journal of biological chemistry* **290**(51): 30453-30463.

Ikeda KN and de Graffenried CL (2012) Polo-like kinase is necessary for flagellum inheritance in Trypanosoma brucei. *Journal of cell science* **125**(Pt 13): 3173-3184.

Inoue M, Okamoto K, Uemura H, Yasuda K, Motohara Y, Morita K, Hiromura M, Reddy EP, Fukuma T and Horikoshi N (2015) Identification and characterization of a cell division-regulating kinase AKB1 (associated kinase of Trypanosoma brucei 14-3-3) through proteomics study of the Tb14-3-3 binding proteins. *J Biochem* **158**(1): 49-60.

Ishida N, Kitagawa M, Hatakeyama S and Nakayama K (2000) Phosphorylation at serine 10, a major phosphorylation site of p27(Kip1), increases its protein stability. *The Journal of biological chemistry* **275**(33): 25146-25154.

Jensen RE and Englund PT (2012) Network news: the replication of kinetoplast DNA. *Annual review of microbiology* **66**: 473-491.

Kabani S, Waterfall M and Matthews KR (2010) Cell-cycle synchronisation of bloodstream forms of Trypanosoma brucei using Vybrant DyeCycle Violet-based sorting. *Molecular and biochemical parasitology* **169**(1): 59-62.

Kall L, Canterbury JD, Weston J, Noble WS and MacCoss MJ (2007) Semi-supervised learning for peptide identification from shotgun proteomics datasets. *Nature methods* **4**(11): 923-925.

Katiyar S, Kufareva I, Behera R, Thomas SM, Ogata Y, Pollastri M, Abagyan R and Mensa-Wilmot K (2013) Lapatinib-binding protein kinases in the african trypanosome: identification of cellular targets for kinase-directed chemical scaffolds. *PloS one* **8**(2): e56150.

Kaufmann D, Gassen A, Maiser A, Leonhardt H and Janzen CJ (2012) Regulation and spatial organization of PCNA in Trypanosoma brucei. *Biochemical and biophysical research communications* **419**(4): 698-702.

Kennedy PGE (2013) Clinical features, diagnosis, and treatment of human African trypanosomiasis (sleeping sickness). *The Lancet Neurology* **12**(2): 186-194.

Kislinger T, Cox B, Kannan A, Chung C, Hu P, Ignatchenko A, Scott MS, Gramolini AO, Morris Q, Hallett MT, Rossant J, Hughes TR, Frey B and Emili A (2006) Global survey of organ and organelle protein expression in mouse: combined proteomic and transcriptomic profiling. *Cell* **125**(1): 173-186.

Kohl L, Robinson D and Bastin P (2003) Novel roles for the flagellum in cell morphogenesis and cytokinesis of trypanosomes. *The EMBO journal* **22**(20): 5336-5346.

Kohl L, Sherwin T and Gull K (1999) Assembly of the paraflagellar rod and the flagellum attachment zone complex during the Trypanosoma brucei cell cycle. *The Journal of eukaryotic microbiology* **46**(2): 105-109.

Lacomble S, Vaughan S, Gadelha C, Morphew MK, Shaw MK, McIntosh JR and Gull K (2009) Three-dimensional cellular architecture of the flagellar pocket and associated cytoskeleton in trypanosomes revealed by electron microscope tomography. *Journal of cell science* **122**(Pt 8): 1081-1090.

Lacomble S, Vaughan S, Gadelha C, Morphew MK, Shaw MK, McIntosh JR and Gull K (2010) Basal body movements orchestrate membrane organelle division and cell morphogenesis in Trypanosoma brucei. *Journal of cell science* **123**(Pt 17): 2884-2891.

Leal S, Acosta-Serrano A, Morita YS, Englund PT, Bohme U and Cross GA (2001) Virulence of Trypanosoma brucei strain 427 is not affected by the absence of glycosylphosphatidylinositol phospholipase C. *Molecular and biochemical parasitology* **114**(2): 245-247.

Leidel S and Gönczy P (2003) SAS-4 Is Essential for Centrosome Duplication in C. elegans and Is Recruited to Daughter Centrioles Once per Cell Cycle. *Developmental cell* **4**(3): 431-439.

Lejon V and Buscher P (2005) Review Article: cerebrospinal fluid in human African trypanosomiasis: a key to diagnosis, therapeutic decision and post-treatment follow-up. *Trop Med Int Health* **10**(5): 395-403.

Li Z (2012) Regulation of the cell division cycle in Trypanosoma brucei. *Eukaryotic cell* **11**(10): 1180-1190.

Licklider LJ, Thoreen CC, Peng J and Gygi SP (2002) Automation of nanoscale microcapillary liquid chromatography-tandem mass spectrometry with a vented column. *Analytical chemistry* **74**(13): 3076-3083.

Liu B, Liu Y, Motyka SA, Agbo EE and Englund PT (2005) Fellowship of the rings: the replication of kinetoplast DNA. *Trends in parasitology* **21**(8): 363-369.

Lundgren DH, Hwang SI, Wu L and Han DK (2010) Role of spectral counting in quantitative proteomics. *Expert Rev Proteomics* **7**(1): 39-53.

Machida YJ and Dutta A (2005) Cellular checkpoint mechanisms monitoring proper initiation of DNA replication. *The Journal of biological chemistry* **280**(8): 6253-6256.

Morriswood B, Havlicek K, Demmel L, Yavuz S, Sealey-Cardona M, Vidilaseris K, Anrather D, Kostan J, Djinovic-Carugo K, Roux KJ and Warren G (2013) Novel bilobe components in Trypanosoma brucei identified using proximity-dependent biotinylation. *Eukaryotic cell* **12**(2): 356-367.

Morriswood B and Schmidt K (2015) A MORN Repeat Protein Facilitates Protein Entry into the Flagellar Pocket of Trypanosoma brucei. *Eukaryotic cell* **14**(11): 1081-1093.

Mutomba MC and Wang CC (1996) Effects of aphidicolin and hydroxyurea on the cell cycle and differentiation of Trypanosoma brucei bloodstream forms. *Molecular and biochemical parasitology* **80**(1): 89-102.

Nishitani H and Lygerou Z (2002) Control of DNA replication licensing in a cell cycle. *Genes Cells* **7**(6): 523-534.

Nolan DP, Geuskens M and Pays E (1999) N-linked glycans containing linear poly-N-acetyllactosamine as sorting signals in endocytosis in Trypanosoma brucei. *Current biology : CB* **9**(20): 1169-1172.

Novak ZA, Wainman A, Gartenmann L and Raff JW (2016) Cdk1 Phosphorylates Drosophila Sas-4 to Recruit Polo to Daughter Centrioles and Convert Them to Centrosomes. *Developmental cell* **37**(6): 545-557.

Ogbadoyi EO, Robinson DR and Gull K (2003) A high-order trans-membrane structural linkage is responsible for mitochondrial genome positioning and segregation by flagellar basal bodies in trypanosomes. *Molecular biology of the cell* **14**(5): 1769-1779.

Okuzumi T, Fiedler D, Zhang C, Gray DC, Aizenstein B, Hoffman R and Shokat KM (2009) Inhibitor hijacking of Akt activation. *Nat Chem Biol* **5**(7): 484-493.

Old WM, Meyer-Arendt K, Aveline-Wolf L, Pierce KG, Mendoza A, Sevinsky JR, Resing KA and Ahn NG (2005) Comparison of label-free methods for quantifying human proteins by shotgun proteomics. *Mol Cell Proteomics* **4**(10): 1487-1502.

Pal A, Hall BS, Nesbeth DN, Field HI and Field MC (2002) Differential endocytic functions of Trypanosoma brucei Rab5 isoforms reveal a glycosylphosphatidylinositol-specific endosomal pathway. *The Journal of biological chemistry* **277**(11): 9529-9539.

Parsons M, Worthey EA, Ward PN and Mottram JC (2005) Comparative analysis of the kinomes of three pathogenic trypanosomatids: Leishmania major, Trypanosoma brucei and Trypanosoma cruzi. *BMC Genomics* **6**: 127.

Patel G, Karver CE, Behera R, Guyett PJ, Sullenberger C, Edwards P, Roncal NE,
Mensa-Wilmot K and Pollastri MP (2013) Kinase scaffold repurposing for
neglected disease drug discovery: discovery of an efficacious, lapatinib-derived
lead compound for trypanosomiasis. *Journal of medicinal chemistry* **56**(10):
3820-3832.

Pelletier L, O'Toole E, Schwager A, Hyman AA and Muller-Reichert T (2006) Centriole
assembly in Caenorhabditis elegans. *Nature* **444**(7119): 619-623.

Portman N and Gull K (2010) The paraflagellar rod of kinetoplastid parasites: from
structure to components and function. *International journal for parasitology* **40**(2):
135-148.

Povelones ML (2014) Beyond replication: Division and segregation of mitochondrial
DNA in kinetoplastids. *Molecular and biochemical parasitology*.

Robinson DR and Gull K (1991) Basal body movements as a mechanism for
mitochondrial genome segregation in the trypanosome cell cycle. *Nature*
352(6337): 731-733.

Robinson DR, Sherwin T, Ploubidou A, Byard EH and Gull K (1995) Microtubule polarity
and dynamics in the control of organelle positioning, segregation, and cytokinesis
in the trypanosome cell cycle. *The Journal of cell biology* **128**(6): 1163-1172.

Schell D, Borowy NK and Overath P (1991) Transferrin is a growth factor for the
bloodstream form ofTrypanosoma brucei. *Parasitology research* **77**(7): 558-560.

Schmidt TI, Kleylein-Sohn J, Westendorf J, Le Clech M, Lavoie SB, Stierhof YD and
Nigg EA (2009) Control of centriole length by CPAP and CP110. *Current biology
: CB* **19**(12): 1005-1011.

Sherwin T and Gull K (1989) The cell division cycle of Trypanosoma brucei brucei: timing of event markers and cytoskeletal modulations. *Philosophical transactions of the Royal Society of London Series B, Biological sciences* **323**(1218): 573-588.

Sheu YJ and Stillman B (2006) Cdc7-Dbf4 phosphorylates MCM proteins via a docking site-mediated mechanism to promote S phase progression. *Molecular cell* **24**(1): 101-113.

Sheu YJ and Stillman B (2010) The Dbf4-Cdc7 kinase promotes S phase by alleviating an inhibitory activity in Mcm4. *Nature* **463**(7277): 113-117.

Siegel TN, Hekstra DR and Cross GA (2008) Analysis of the Trypanosoma brucei cell cycle by quantitative DAPI imaging. *Molecular and biochemical parasitology* **160**(2): 171-174.

Singec I, Crain AM, Hou J, Tobe BT, Talantova M, Winquist AA, Doctor KS, Choy J, Huang X, La Monaca E, Horn DM, Wolf DA, Lipton SA, Gutierrez GJ, Brill LM and Snyder EY (2016) Quantitative Analysis of Human Pluripotency and Neural Specification by In-Depth (Phospho)Proteomic Profiling. *Stem Cell Reports* **7**(3): 527-542.

Steverding D, Stierhof Yd Fau - Chaudhri M, Chaudhri M Fau - Ligtenberg M, Ligtenberg M Fau - Schell D, Schell D Fau - Beck-Sickinger AG, Beck-Sickinger Ag Fau - Overath P and Overath P ESAG 6 and 7 products of Trypanosoma brucei form a transferrin binding protein complex. (0171-9335 (Print)).

Takadate T, Onogawa T, Fukuda T, Motoi F, Suzuki T, Fujii K, Kihara M, Mikami S, Bando Y, Maeda S, Ishida K, Minowa T, Hanagata N, Ohtsuka H, Katayose Y,

Egawa S, Nishimura T and Unno M (2013) Novel prognostic protein markers of resectable pancreatic cancer identified by coupled shotgun and targeted proteomics using formalin-fixed paraffin-embedded tissues. *International Journal of Cancer* **132**(6): 1368-1382.

Tanaka S, Umemori T, Hirai K, Muramatsu S, Kamimura Y and Araki H (2007) CDK-dependent phosphorylation of Sld2 and Sld3 initiates DNA replication in budding yeast. *Nature* **445**(7125): 328-332.

Taus T, Kocher T, Pichler P, Paschke C, Schmidt A, Henrich C and Mechtler K (2011) Universal and confident phosphorylation site localization using phosphoRS. *Journal of proteome research* **10**(12): 5354-5362.

Tiengwe C, Marques CA and McCulloch R (2014) Nuclear DNA replication initiation in kinetoplastid parasites: new insights into an ancient process. *Trends in parasitology* **30**(1): 27-36.

Traxler P, Allegrini PR, Brandt R, Brueggen J, Cozens R, Fabbro D, Grosios K, Lane HA, McSheehy P, Mestan J, Meyer T, Tang C, Wartmann M, Wood J and Caravatti G (2004) AEE788: a dual family epidermal growth factor receptor/ErbB2 and vascular endothelial growth factor receptor tyrosine kinase inhibitor with antitumor and antiangiogenic activity. *Cancer research* **64**(14): 4931-4941.

Tu X, Mancuso J, Cande WZ and Wang CC (2005) Distinct cytoskeletal modulation and regulation of G1-S transition in the two life stages of Trypanosoma brucei. *Journal of cell science* **118**(Pt 19): 4353-4364.

Tu X and Wang CC (2004) The involvement of two cdc2-related kinases (CRKs) in Trypanosoma brucei cell cycle regulation and the distinctive stage-specific phenotypes caused by CRK3 depletion. *The Journal of biological chemistry* **279**(19): 20519-20528.

Tu X and Wang CC (2005) Pairwise knockdowns of cdc2-related kinases (CRKs) in Trypanosoma brucei identified the CRKs for G1/S and G2/M transitions and demonstrated distinctive cytokinetic regulations between two developmental stages of the organism. *Eukaryotic cell* **4**(4): 755-764.

Ulery PG, Rudenko G and Nestler EJ (2006) Regulation of DeltaFosB stability by phosphorylation. *J Neurosci* **26**(19): 5131-5142.

Vazquez F, Ramaswamy S, Nakamura N and Sellers WR (2000) Phosphorylation of the PTEN tail regulates protein stability and function. *Molecular and cellular biology* **20**(14): 5010-5018.

Wan X, Harkavy B, Shen N, Grohar P and Helman LJ (2007) Rapamycin induces feedback activation of Akt signaling through an IGF-1R-dependent mechanism. *Oncogene* **26**(13): 1932-1940.

Wang SA, Hung CY, Chuang JY, Chang WC, Hsu TI and Hung JJ (2014) Phosphorylation of p300 increases its protein degradation to enhance the lung cancer progression. *Biochimica et biophysica acta* **1843**(6): 1135-1149.

Woodward R and Gull K (1990) Timing of nuclear and kinetoplast DNA replication and early morphological events in the cell cycle of Trypanosoma brucei. *Journal of cell science* **95 (Pt 1)**: 49-57.

Xie X, Feng S, Vuong H, Liu Y, Goodison S and Lubman DM (2010) A comparative phosphoproteomic analysis of a human tumor metastasis model using a label-free quantitative approach. *Electrophoresis* **31**(11): 1842-1852.

Yamamoto H, Kishida S, Kishida M, Ikeda S, Takada S and Kikuchi A (1999) Phosphorylation of axin, a Wnt signal negative regulator, by glycogen synthase kinase-3beta regulates its stability. *The Journal of biological chemistry* **274**(16): 10681-10684.

Zhang B, VerBerkmoes NC, Langston MA, Uberbacher E, Hettich RL and Samatova NF (2006) Detecting differential and correlated protein expression in label-free shotgun proteomics. *Journal of proteome research* **5**(11): 2909-2918.

Zhang F, Phiel CJ, Spece L, Gurvich N and Klein PS (2003) Inhibitory phosphorylation of glycogen synthase kinase-3 (GSK-3) in response to lithium. Evidence for autoregulation of GSK-3. *The Journal of biological chemistry* **278**(35): 33067-33077.

Zhou Q, Gheiratmand L, Chen Y, Lim TK, Zhang J, Li S, Xia N, Liu B, Lin Q and He CY (2010) A comparative proteomic analysis reveals a new bi-lobe protein required for bi-lobe duplication and cell division in Trypanosoma brucei. *PloS one* **5**(3): e9660.

Zhou Q, Hu H and Li Z (2014) New insights into the molecular mechanisms of mitosis and cytokinesis in trypanosomes. *International review of cell and molecular biology* **308**: 127-166.

Zou L and Stillman B (2000) Assembly of a complex containing Cdc45p, replication protein A, and Mcm2p at replication origins controlled by S-phase cyclin-

dependent kinases and Cdc7p-Dbf4p kinase. *Molecular and cellular biology*

20(9): 3086-3096.

Footnotes

Figure Legends

Figure 1. *AEE788 blocks kinetoplast elongation and division*. Trypanosomes (5×10^5 cells/ml) were treated with AEE788 (5 μM) or DMSO (0.1%), in HMI-9 medium, for 4 h. Cells were fixed in paraformaldehyde and the kinetoplast and nuclear DNA stained with DAPI. The number of kinetoplasts and nuclei in 150 trypanosomes were quantitated. (**A**) Representative images of DAPI-stained trypanosomes after treatment with DMSO (top) or AEE788 (bottom). The scale bar is 6 μm. (**B**) The average percentage of trypanosomes within each kinetoplast (K) and nucleus (N) configuration are shown. Ke = elongated kinetoplast. Error bars represent standard deviation between 4 biological replicates. The distribution of kinetoplasts and nuclei (per trypanosome) in DMSO-treated and AEE788-treated cells was compared using a Pearson chi-squared test ($p = 7.4 \times 10^{-19}$).

Figure 2. *AEE788 decreases DNA synthesis in the kinetoplast and nucleus*. Trypanosomes were treated with AEE788 (5 μM) or DMSO (0.1%) for 4 h. 5-ethynyl-2'-deoxyuridine (EdU) and 2'-deoxycytidine were added to both cultures during the last 30 minutes of treatment. Incorporated EdU was detected in a click-iT reaction with a fluorescent azide. (**A**) Kinetoplasts (K) and nuclei (N) were scored as EdU-positive (K+ or N+) or EdU-negative after treatment with DMSO (top) or AEE788 (bottom). The scale bar is 10 μm. (**B**) Quantitation of the average percentage of trypanosomes (n = 125) with EdU-negative or EdU-positive kinetoplasts following AEE788 or DMSO treatment. (**C**) Quantitation of the average proportion of cells (n = 125) with EdU-negative or EdU-positive nuclei following AEE788 or DMSO treatment. Error bars denote the standard deviation in three independent experiments. Differences in the distribution of trypanosomes between EdU-positive and EdU-negative kinetoplasts or nuclei in cell populations treated with DMSO or AEE788 were assessed with a Pearson chi-squared test ($p = 4.9 \times 10^{-4}$ for the kinetoplast, and $p = 3.1 \times 10^{-19}$ for the nucleus).

Figure 3. *AEE788 prevents basal body duplication*. Anti-TbSAS6 and YL1/2 were used to quantitate the number of mature basal bodies (mBB) and immature probasal bodies (pBB) per trypanosome after treatment with AEE788 (5 µM) or DMSO (0.1%). (**A**) Representative staining pattern of YL1/2 (red) and anti-TbSAS6 (green) after DMSO (top) or AEE788 (bottom) treatment. Cells are counterstained with DAPI (1.5 µM). Red arrows indicate TbRP2+ foci (mBB), green arrows indicate TbSAS6+ foci (pBB), and yellow arrows indicate colocalization of TbRP2 and TbSAS6 (mBB). The scale bar is 6 µm. The basal bodies and associated kinetoplast (K) are enlarged in a single trypanosome for both treatment groups: DMSO (yellow boxes) and AEE788 (orange boxes). (**B**) Average percentage of trypanosomes (n = 125) with the indicated number of mBBs and pBBs following treatment with AEE788 or DMSO. Error bars represent the standard deviation in three independent experiments. Statistical significance of changes in the distribution of the number of basal bodies (per cell) in the trypanosome population was determined with a Pearson chi-squared test ($p = .3 \times 10^{-18}$).

Figure 4. *Bilobe duplication is inhibited by AEE788*. Following a 4 h treatment with AEE788 (5 µM) or DMSO (0.1%), trypanosomes were stained with the anti-centrin antibody 20H5 to detect the bilobe. (**A**) Representative images of 20H5-stained trypanosomes after treatment with DMSO (top) or AEE788 (bottom). Centrin is observed at the bilobe (green arrowheads) as well as the basal body (green arrows). DAPI was used to stain kinetoplast and nuclear DNA. K = kinetoplast; N = nucleus. The scale bar is 6 µm. (**B**) Average percentage of cells with one or two bilobes following AEE788 or DMSO treatment. Error bars represent standard deviation between four biological replicates. The distribution of trypanosomes with one or two bilobes in AEE788-treated cells was compared to the distribution observed in control cells (i.e. DMSO-treated) using a Pearson chi-squared test ($p = 3.6 \times 10^{-9}$).

Figure 5. *Time-course of DNA replication and division in the kinetoplast and nucleus after withdrawal of AEE788*. Trypanosomes were treated with AEE788 (5 μM, 4 h), rinsed, and placed in drug-free HMI-9 medium. The time-course of DNA synthesis was monitored by EdU incorporation and DAPI was used to visualize division of the kinetoplast and nucleus. (**A**) Representative images of trypanosomes directly after AEE788 treatment (0 h, top panel) or 2 h after AEE788 washout (bottom). Kinetoplasts and nuclei, in 100-150 trypanosomes, were scored as EdU-positive (K+ or N+) or EdU-negative. Ke = elongated kinetoplast. Scale bar = 15 μm. The average proportion of cells with EdU-positive kinetoplasts (**B**), or nuclei (**C**), are indicated at every hour following AEE788 withdrawal. Standard deviation between independent experiments are shown (n = 6 for 0 h and 2 h; n = 4 for 1 h; n = 3 for 3 h and 4 h). A sigmoidal nonlinear regression curve was fit to the data points using GraphPad Prism, and the time at which 10% (T_{10}) or 50% (T_{50}) of the population became EdU-positive, compared to the observed maximum (4 h), was calculated for kinetoplast (**B**) and nuclear (**C**) EdU incorporation. (**D**) The average percentage of cells (n = 115) with the indicated kinetoplast (K) and nucleus (N) configuration is shown for every hour after AEE788 withdrawal. Standard deviation represents variation between three independent experiments. Data trends are represented by nonlinear regression curves using a 3rd order polynomial equation for 1K1N and 1Ke1N data, and a sigmoidal nonlinear regression curve for 2K1N and 2K2N populations. T_{10} and T_{50} (calculated by GraphPad software) for each event is listed. (T_{10} and T_{50} for the appearance of 1Ke1N cells is based on a sigmoidal nonlinear regression curve from 0 h to 4 h (maximum)).

Figure 6. *Kinetics of basal body and bilobe duplication*. Trypanosomes were treated with AEE788 (5 μM, 4 h) and then transferred to drug-free HMI-9 medium for up to 3 h. Cells were retrieved every 30 minutes between 2 h and 3 h after AEE788 washout (**A**) Basal body duplication was assessed with YL1/2 and anti-TbSAS6. YL1/2 recognizes mature basal bodies (mBBs) (red arrows) and TbSAS6 localizes to immature probasal bodies (pBB) (green arrows) and mature

basal bodies (yellow arrows). The scale bar is 6 μm. An unduplicated basal body (1mBB/1pBB) 1.5 h after AEE788 washout (yellow boxes) and a duplicated basal body (2mBB/2pBB) 3 h after AEE788 washout (orange boxes) are magnified. K = kinetoplast. (***B***) The average percentage of cells with the indicated number of mature basal bodies (mBB) and probasal bodies (pBB) are shown at various times after AEE788 washout. Error bars represent standard deviation between three independent experiments. A sigmoidal nonlinear regression curve was fit to the data points in GraphPad Prism and the time by which 10% (T_{10}) or 50% (T_{50}) of the population, compared to the observed maximum, became 2mBB/2pBB, is listed. (***C***) Schematic of nascent basal body duplication and probasal body maturation (acquisition of TbRP2) occurring in the absence of intermediates with two mature basal bodies and no probasal bodies (2mBB/0pBB). (***D***) The anti-centrin antibody, 20H5, was used to visualize bilobes. Green arrowheads indicate bilobes, green arrows point to basal bodies. K = kinetoplast; N = nucleus. Scale bar is 10 μm. (***E***) Quantitation of the average percentage of bilobes (BL) per cell following AEE788 withdrawal. Error bars represent standard deviation between three independent experiments. A sigmoidal nonlinear regression curve was fit to the data points in GraphPad Prism, and the T_{10} and T_{50}, describing the formation of cells with duplicated bilobes, are provided.

Figure 7. *Time-course of major events in the trypanosome division cycle*. AEE788 (5 μM, 4 h) was used to block organelle duplication and DNA synthesis. After removing AEE788 from the medium, the onset and duration of organelle duplication and DNA synthesis were determined. The time at which, 10% (T_{10}) (left border), 50% (T_{50}) and 90% (T_{90}) (right border) of the observed maximum was reached for each event was calculated, based on nonlinear regression curves (Figures 5 and 6). The darkest shading corresponds to the T_{50} (+/- standard error).

Figure 8. *Extended AEE788 exposure decreases trypanosome viability*. Trypanosomes were treated with AEE788 (5 μM) or DMSO (0.1%) for 4 h, 9 h or 16 h, harvested and treated with

propidium iodide (3 µM) prior to analysis on a flow cytometer. Trypanosomes were gated based

on size and shape (forward and side scatter) and the intensity of propidium iodide (PI) determined.

Figure 9. *Effect of AEE788 on endocytic pathways*. Trypanosomes (5 x 10^5 cells/ml) were

incubated with AEE788 (5 µM) or DMSO (0.1%) for 9 h. Cells were subsequently washed and

resuspended in serum-free medium (without drug or DMSO). Trypanosomes were incubated with

fluorescent endocytic cargo (transferrin, BSA, or tomato lectin) for 15 minutes (37 °C). Propidium

iodide (3 µM) was used to stain dead cells. A flow cytometer was used to detect fluorescence

intensity per cell. (**A**) FlowJo software was used to gate for live trypanosomes based on shape

(forward and side scatter) and ability to exclude propidium iodide. Histograms depict fluorescence

intensity for transferrin (**B**), BSA (**C**) or tomato lectin (**D**) for every observed cell (n = 15,000 for

each cargo). Bar graphs represent the average median fluorescence intensity (calculated with

FloJo), with standard deviation between three independent experiments shown, for transferrin

(**B**), BSA (**C**) or tomato lectin (**D**) after DMSO or AEE788 treatment. In statistical analysis, the

median fluorescence of each cargo was compared between cells treated with DMSO or AEE788

using a Student's t-test ($p = 0.002$ for Tf, $p = 0.003$ for BSA and $p = 0.9$ for TL).

Figure 10. *Prolonged AEE788 exposure changes trypanosome morphology.* (**A**) The morphology

of live trypanosomes (n = 100) was determined after different durations of AEE788 treatment

(examples of trypanosome morphology are demonstrated by paraformaldehyde fixed cells). The

standard deviation of two experiments is shown. A Pearson chi-squared test was used to compare

the distribution of normal, swollen and rounded cells between different treatment groups; 4 h to 9

h ($p = 6.6$ x 10^{-64}); 4 h to 16 h ($p = 1.1$ x 10^{-64}); 9 h to 16 h ($p = 5.6$ x 10^{-25}). (**B**) Following a 16 h

treatment with DMSO (top) or AEE788 (bottom), the paraflagellar rod (PFR) was visualized using

an antibody against PFR2 (green) and the flagellum with the antibody 20H5 (red). 20H5 detects

centrin at the basal body (arrow), bilobe (arrowhead) and the flagellum. K = kinetoplast; N =

nucleus. The scale bar is 6 μm. (**C**) Trypanosomes were treated with AEE788 (5 μM) for 12 h and visualized by SEM. The left panel demonstrates normal trypanosome morphology, the middle panel shows both rounded (left) and swollen (right) cells, and the right panel depicts a round trypanosome with flagellum at the cell periphery (white arrow). The scale bar is 2 μm.

Table 1. *Select examples of phosphoproteins affected by short-term (4 h) AEE8788 treatment. After treatment of trypanosomes with DMSO (0.1%) or AEE788 (5 μM) for 4 h, peptides were harvested and phosphopeptides enriched over an IMAC column. LC-MS/MS was used to monitor the abundance of phosphopeptides in three independent experiments. Spectral counts indicate the combined number of times a phosphopeptide was observed over all experiments. The number in parenthesis indicates the total number of peptides observed for the parent protein over all experiments (summation of all peptides observed in the IMAC elution and flow through). The affected peptide is indicated with the phosphosite bolded in lowercase (phosphoRS (Taus et al., 2011) probability ≥ 80%). A Student's t-test was used to determine if the change in phosphopeptide abundance was statistically significant (p < 0.05%).*

Gene ID	Production Description	Identified Phosphopeptide	Spectral Counts		*p*-value
			DMSO	**AEE788**	
Decreased					
Tb427.06.4970	SR Protein Kinase (SRPK)	Hs**ASTNGPSQPAHQR**	**6** (15)	**1** (3)	0.038
Tb427.10.3010	Bilobe Protein	**s**RISTGISFLSK	**5** (18)	**0** (7)	0.038
Tb427tmp.02.0810	TbSAS4	LAVGDANHSESIGDKSVst**K**	**8** (12)	**2** (3)	0.013
Increased					
Tb427.01.2100	Calpain-like Cysteine Peptidase	AEEASPAPSPAGE**s**DEKAs**K**SEHESEAK	**20** (88)	**44** (99)	0.03

59

Table 2. *Select examples of phosphoproteins affected by long-term (9 h) AEE8788 treatment. After treatment of trypanosomes with DMSO (0.1%) or AEE788 (5 μM) for 4 h, trypanosome phosphopeptides were enriched over an IMAC column. Phosphopeptide abundance was monitored by LC-MS/MS in three independent experiments. Spectral counts indicate the combined number of times a phosphopeptide was observed over all three experiments. The number in parenthesis indicates the total number of peptides observed for the parent protein over all experiments (summation of all peptides observed in the IMAC elution and flow through). The affected peptide is indicated with the phosphosite bolded in lowercase (phosphoRS (Taus et al., 2011) probability ≥ 80%). A Student's t-test was used to determine if the change in phosphopeptide abundance was statistically significant ($p < 0.05\%$).*

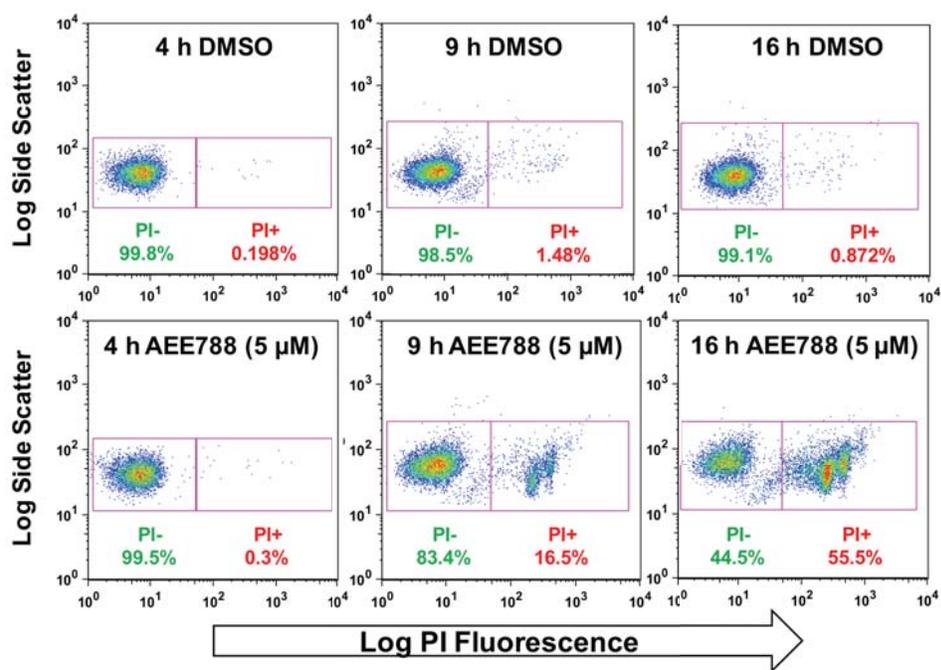| Gene ID	Production Description	Identified Phosphopeptide	Spectral Counts		p-value
			DMSO	**AEE788**	
Decreased					
Tb427.03.3080	NEK Kinase	ADT**s**DI**s**LSHEDL**s**R	**12** (16)	**0** (7)	0.02
Tb427.10.14010	TbRP2	EATPPE**s**ASRSDSSAPTTPHSR	**8** (25)	**1** (7)	0.05
Tb427.10.8820	Bilobe Protein	TIGTTSGHSTTNL**ss**HTPEK	**6** (17)	**0** (5)	0.03
Tb427tmp.01.3960	BILBO-1	LMSEAS**s**FLGNLR	**5** (41)	**0** (26)	0.04
Increased					
Tb427.10.14770	Associated kinase of Tb14-3-3	LANS**s**LPV**s**HTSTR	**7** (13)	**15** (18)	0.02
Tb427.07.7000	Bilobe Protein	TSSHI**s**EHGLDR	**0** (38)	**10** (67)	0.02
Tb427.04.310	Ubiquitin-transferase	TTLSKsAHV**s**HER	**3** (3)	**8** (9)	0.04
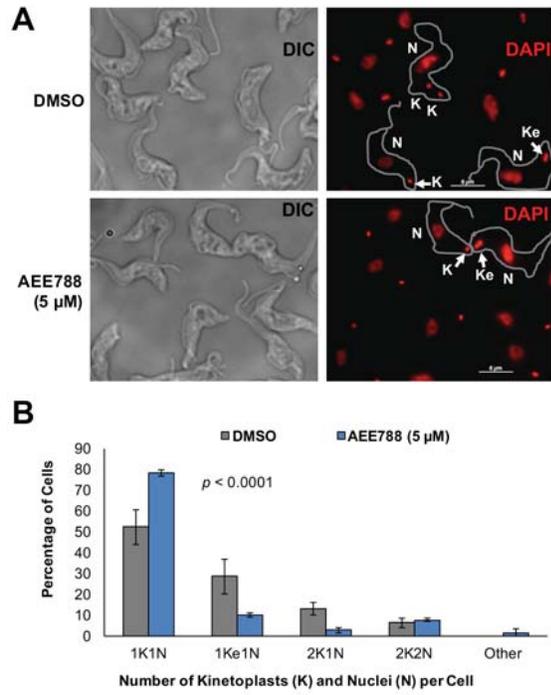
Figure 1
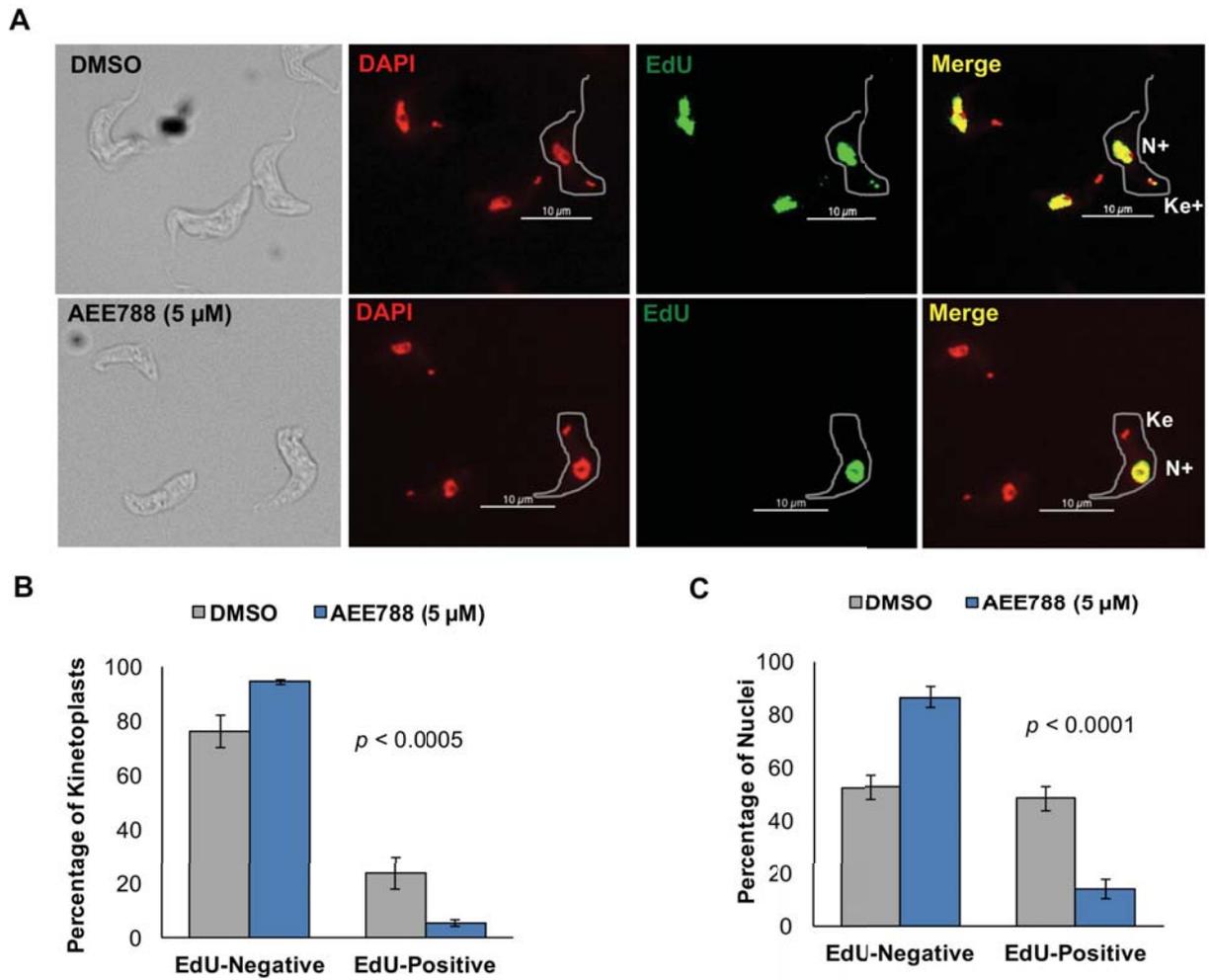
Figure 2
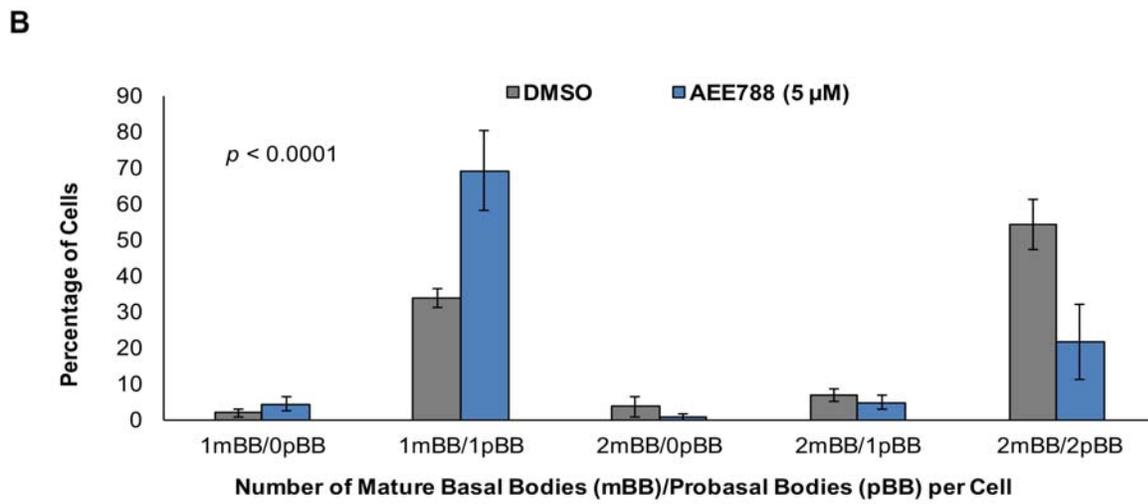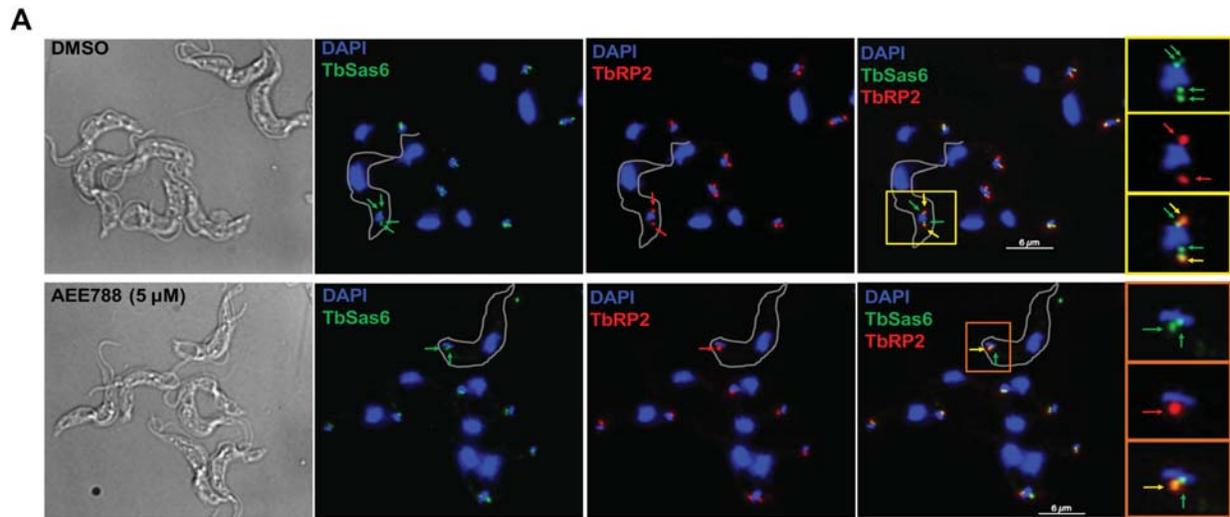
Figure 3
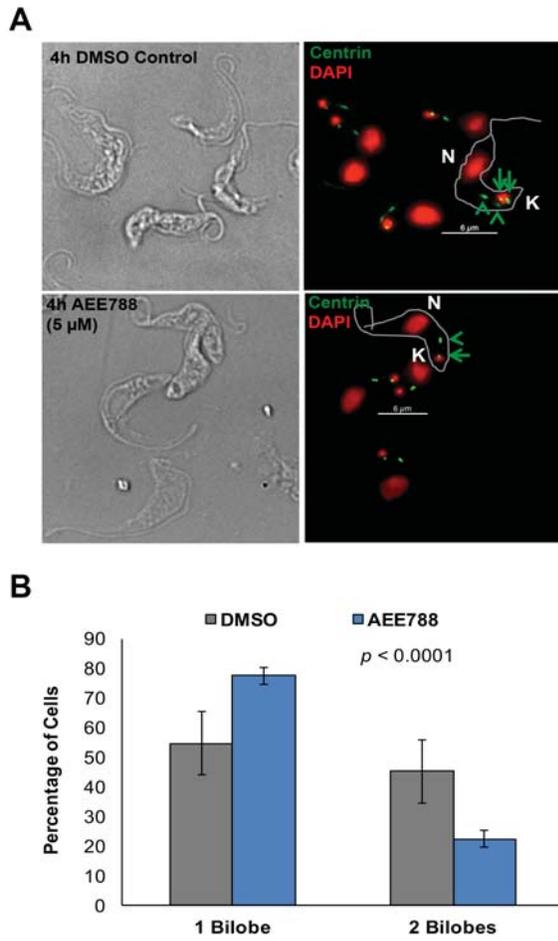
Figure 4
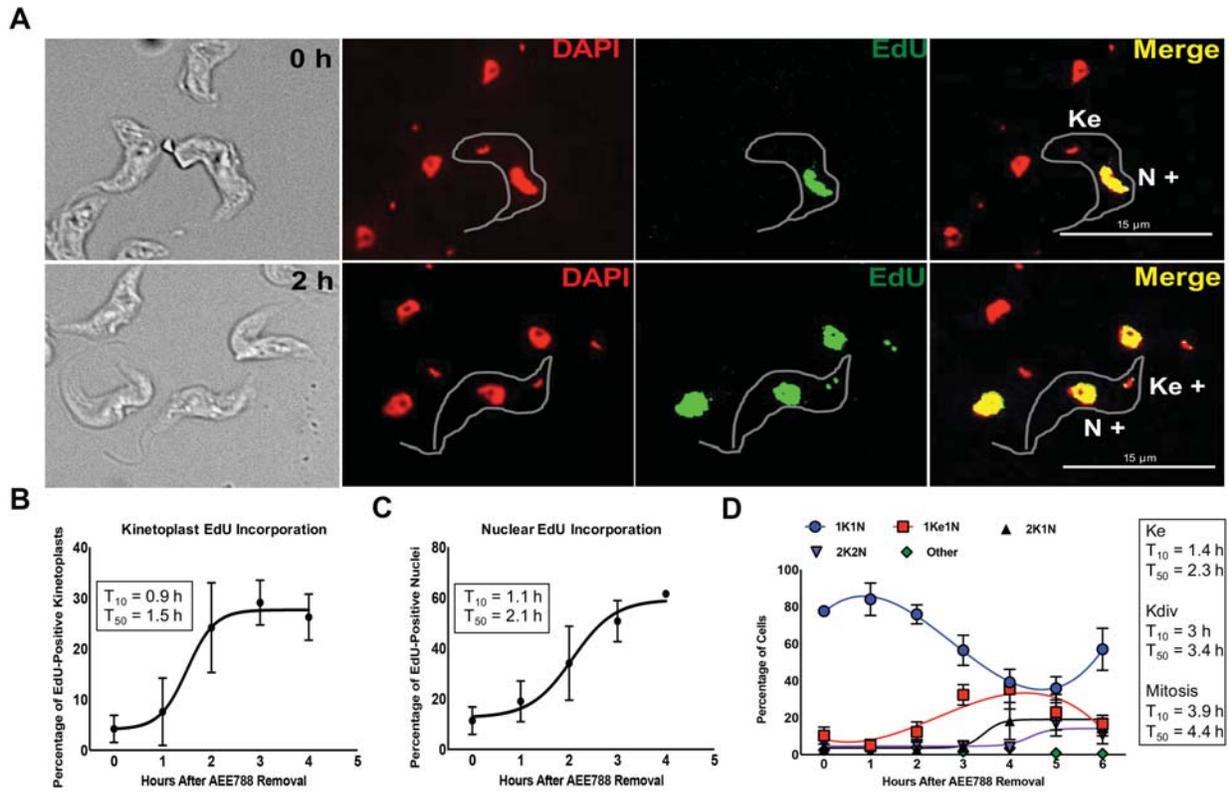
Figure 5
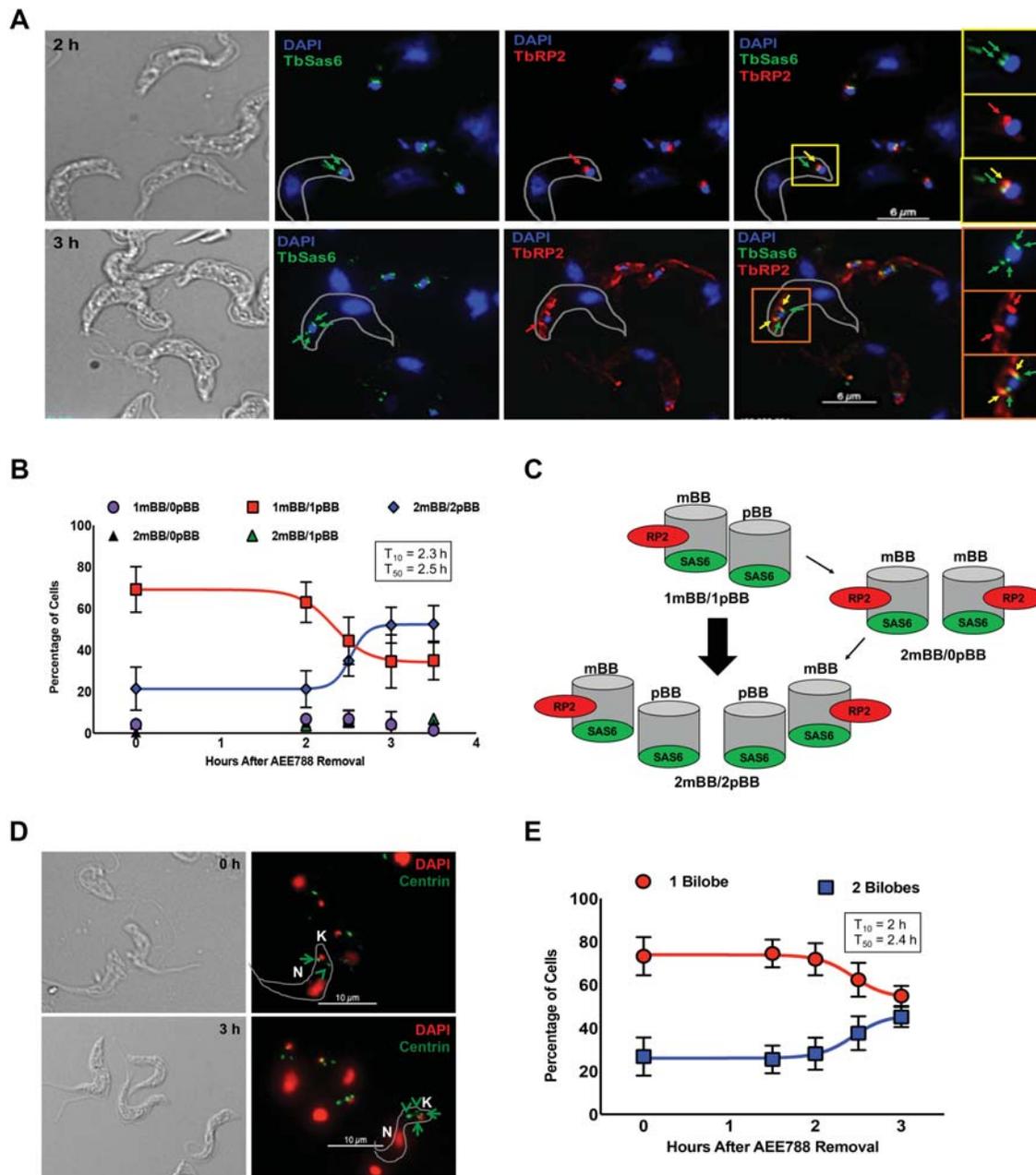
Figure 6
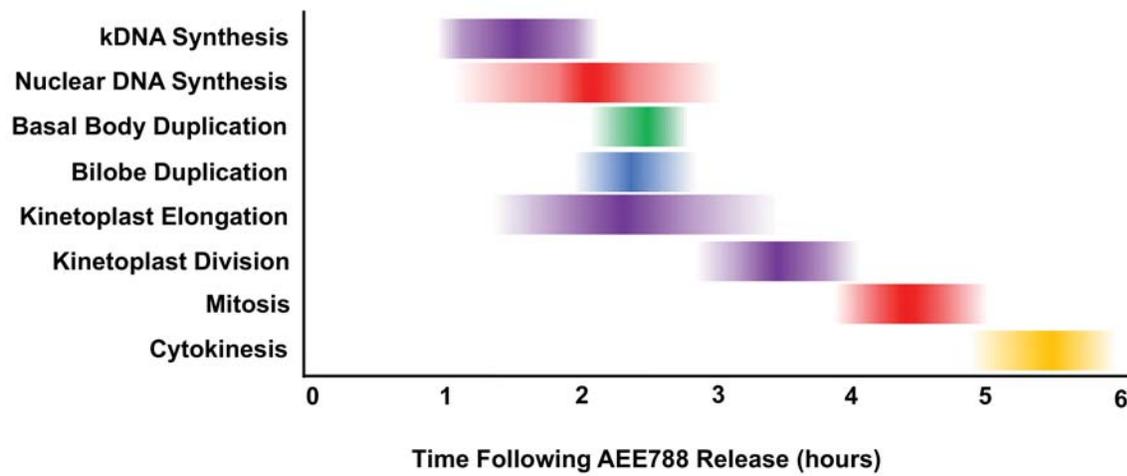
Figure 7

Figure 8

Figure 9

Figure 10